Electronic Supplementary Information

Cofacial Porphyrin Organic Cages. Metals Regulating Excitation Electron Transfer and CO_2 Reduction Electrocatalytic Properties

Xiaolin Liu,[a] Chenxi Liu,[a] Xiaojuan Song,[b] Xu Ding,[a] Hailong Wang,*[a] Baoqiu Yu,[a] Heyuan Liu,*[b] Bin Han,[a] Xiyou Li,*[b] and Jianzhuang Jiang*[a]

[a] X. Liu, C. Liu, X. Ding, Prof. H. Wang, B. Yu, Dr. B. Han, Prof. J. Jiang
Beijing Advanced Innovation Center for Materials Genome Engineering, Beijing Key Laboratory for Science and Application of Functional Molecular and Crystalline Materials, Department of Chemistry and Chemical Engineering, School of Chemistry and Biological Engineering
University of Science and Technology Beijing, Beijing 100083, China
E−mail: hlwang@ustb.edu.cn (H.W.) and jianzhuang@ustb.edu.cn (J.J.)

[b] X. Song, Dr. H. Liu, Prof. X. Li
School of Materials Science and Engineering
China University of Petroleum (East China), Qingdao 266580, China
E−mail: 20170053@upc.edu.cn(H.L.) and xiyouli@upc.edu.cn (X.L.)

Table of Contents

Experimental Procedures

General Information. All other regents were commercially available and directly employed. The synthesis of *meso*−tetra(*p*−formylphenyl)porphyrin was referred to the previous literature procedure with slight modifications.

Synthesis of *meso*−tetra(*p*−formylphenyl)porphyrin.

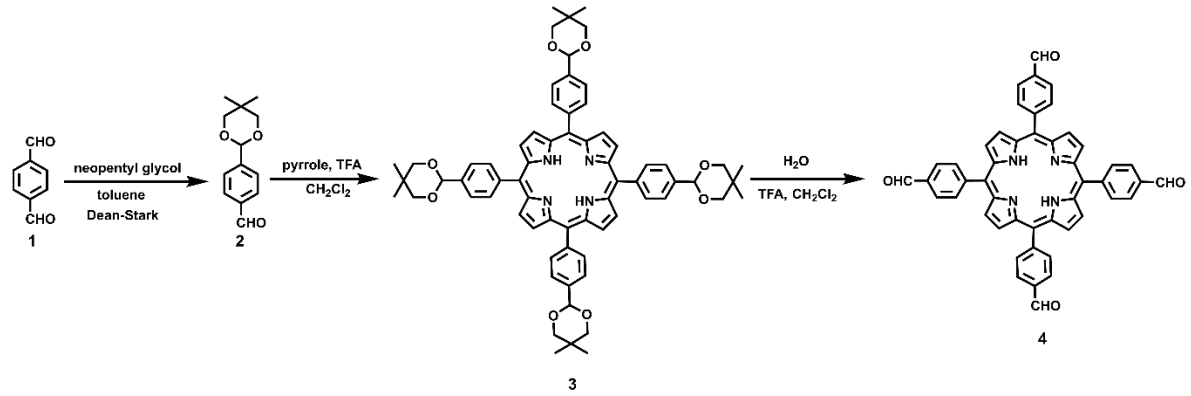

Scheme S1 Schematic synthesis of meso−Tetra(p−formylphenyl)porphyrin (**4**).

Synthesis of 4−(5,5−dimethyl−1,3−dioxan−2−yl)benzaldehyde (2).[S1] To a solution of terephthalaldehyde **1** (5.0 g, 37.3 mmol) in toluene (100 mL) was added 2,2-dimethyl-1,3-propanediol (4.3 g, 41.0 mmol) followed by adding a catalytic amount of *p*−toluenesulfonic acid (PTSA, 10.0 mg). The reaction mixture was refluxed 5 h with a Dean−Stark. The progress of the reaction was monitored by TLC (EtOAc/hexane = 2:8 v/v). The reaction solution was concentrated under vacuum and the crude compound was purified by silica gel column chromatography to give **2** (5.9 g, 71.4 %) as a white solid. ^{1}H NMR (400 MHz, $CDCl_3$): δ (ppm) 10.03 (s, 1H), 7.89 (d, 2H), 7.68 (d, 2H), 5.45 (s, 1H), 3.79 (d, 2H), 3.67 (d, 2H),1.29 (s, 3H), 0.82 (s, 3H).

Synthesis of tetrakis[4−(1,3−dioxa−5,5−dimethylcyclohex−2−yl)phenyl]porphyrin (3).[S1] A solution of pyrrole (348.0 µL, 5.0 mmol) and **2** (1.1 g, 5.0 mmol) in dry dichloromethane (500 mL) was purged with nitrogen for 30 min. To this solution trifluoroacetic acid (386.0 µL, 5.0 mmol) was added. The reaction mixture (protected from light) was stirred at 45 °C for 2 h under nitrogen atmosphere. To this resulting black color solution, 1,2-dichloro-4,5-dicyanobenzoquinone (0.9 g, 5.0 mmol) was added, continue stirring for 0.5 h. After cooling down to room temperature, the resulting reaction mixture was concentrated in vacuo to 1/4 by volume. The concentrated solution was then filtered through a bed of deactivated neutral alumina and eluted with dichloromethane until disappearance of the violet filtrate was observed. The combined organic phase was evaporated to dryness and the residue was purified by silica gel column chromatography eluting with dichloromethane to give compound **3**. Yield: 0.27 g (20.2%). ^{1}H NMR (400 MHz, $CDCl_3$): δ (ppm) 8.82 (s, 8H), 8.21 (d, 8H), 7.91 (d, 8H), 5.76 (s, 4H), 3.96 (d, 8H), 3.86 (d, 8H), 1.47 (s, 12H), 0.92 (s, 12H), −2.84 (s, 2H).

Synthesis of *meso*−tetra(*p*−formylphenyl)porphyrin(4). Trifluoroacetic acid (50.0 mL) was added to a solution of tetrakis[4−(1,3−dioxa−5,5−dimethylcyclohex−2−yl)phenyl]porphyrin (500 mg, 0.5 mmol) in dichloromethane (50 mL) and water (50 mL). After stirred (protected from light) at room temperature overnight under N_2 atmosphere, 20 mL trifluoroacetic acid was replenished to the mixture and then stirred for additional 12 h. Then the TFA in the solution was neutralized with aqueous K_2CO_3 solution and washed with water three times. The organic layer was separated, dried over anhydrous K_2CO_3 and evaporated in vacuum. The crude

product was purified by column chromatography on silica gel (CH_2Cl_2: MeOH = 99:1 v/v) to afford *meso*−tetra(*p*−formylphenyl)porphyrin as violet crystal with the yield of 85.8% (291 mg). ^{1}H NMR (400 MHz, $CDCl_3$): δ (ppm) 10.4 (s, 4H), 8.84 (s, 8H), 8.40 (d, 8H), 8.30 (d, 8H), −2.78 (s, 2H).

Synthesis of ANDI. chiral (2−aminocyclohexyl)−1,4,5,8−naphthalenetetraformyl diimide (ANDI) was synthesized following the previous literature.[S2]

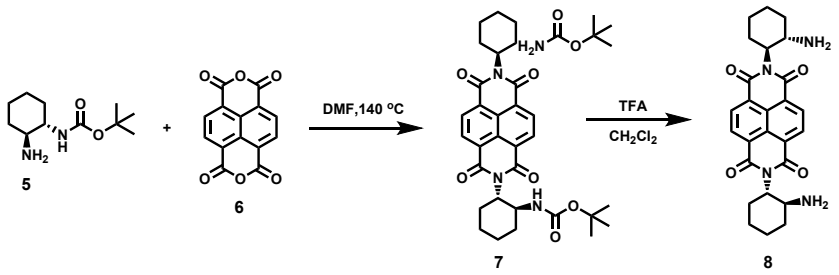

Scheme S2 Schematic synthesis of (S)−and (R)−Naphthalene−1,4:5,8−bis(dicarboximide) (**8**).

Synthesis of protected NDI diamine (7). The di-tert butyl dicarbonate (BOC) protected chiral cyclohexanediamine **5** (2.6 g, 12.3 mmol) was dissolved in dry DMF (140 ml). **6** (1.5 g, 5.6 mmol) was added and the resulting mixture was stirred at 140°C for 17 hours under nitrogen atmosphere. The solvent was removed under reduced pressure. The residue was dry-loaded on silica and purified by column chromatography on silica using hexanes/EtOAc (3:1) as eluent to afford the pure product (2.8 g, 91.2%) as a yellowish to grey-yellowish solid. ^{1}H NMR (400 MHz, $CDCl_3$): δ 8.71 – 8.76 (s, 4H), 4.85 (ddd, 2H), 4.54 (s, 2H), 4.39 (s, 2H), 2.78 (s, 2H), 2.15 (dd, 2H), 1.89 (d, 2H), 1.83 (d, 4H), 1.57 – 1.45 (m, 2H), 1.44 – 1.33 (m, 2H), 1.32 – 1.21 (m, 2H), 0.88 (s, 18H).

Synthesis of ANDI. (8). The **7** (0.8 g, 1.5 mmol) was dissolved in the mixture of CH_2Cl_2/TFA (60 ml, 1:1 v/v) and the resulting solution was stirred at room temperature for 5 h. The solvent was removed under reduced pressure. The white solid that was obtained was suspended in brine and sat. NH_4OH was added to reach pH of 12. The color of the solids turned to slightly yellow and the mixture was extracted with several portions of chloroform. Combined organic layers were washed with brine, dried with Na_2SO_4 and the solvent was removed under reduced pressure to yield the pure product (0.55 mg, 81.45%) as a yellowish solid. ^{1}H NMR (400 MHz, $CDCl_3$): δ 8.72 (m, 4H), 4.77 (m, 2H), 3.74 (m, 2H), 2.50 (m, 2H), 2.10 (m, 2H), 1.89 – 1.80 (m, 6H), 1.52 – 1.43 (m, 2H), 1.32 – 1.26 (m, 4H).

Synthesis of CPOC−H_2. To a solution of *meso*−tetra(*p*−formylphenyl)porphyrin (100.0 mg, 0.14 mmol) and ANDI (322.1 mg, 0.7 mmol, 5 eq) in $CHCl_3$ (150 mL), a catalytic amount of TFA (30.0 µL) was added. After stirred at 70°C for 10 h, the solvent was evaporated under reduced pressure. Recrystallization from $CHCl_3$ / MeOH afforded a brownish red solid with the yield of (173.7 mg) 80.1 %. ^{1}H NMR ($CDCl_3$, 400 MHz): δ 8.81 (q, 16 H), 8.54 (s, 8 H), 8.23 (d, 8 H), 8.21 (d, 8 H),8.08 (d, 8 H), 7.98 (d, 8 H), 7.41 (d, 8H), 6.93 (d, 8H), 5.56 − 5.49 (m, 8 H), 4.75 − 4.70 (m, 8 H), 2.67 (t, 8 H), 2.11 − 1.94 (m, 40 H), 1.76 − 1.60 (m, 16 H), −2.7 − −3.3 (m, 4H). MALDI-TOF (m/z): $[M]^+$ 3150.2, found 3150.8.

Synthesis of CPOC−Co. CPOC−H_2 organic cage (32.0 mg, 0.01 mmol) was dissolved in a mixed solvent of chloroform (60 mL) and methanol (20 mL), then the cobalt acetate (35.4 mg, 0.2 mmol) was added in this reactor, the solution was stirred at room temperature for overnight, then washed with several portions of methanol, and dried over Na_2SO_4. Evaporation of the solvent gave 27.9 mg of a maroon solid with 84.2% yield. Since the cobalt metal at the center of the porphyrin contains a single electron which is a paramagnetic metal ion, accurate nuclear magnetic data cannot be obtained. The progress of the reaction was monitored by Uv-vis spectrum. MALDI-TOF (m/z): $[M]^+$ 3263.0, found 3263.8.

Synthesis of CPOC−Ni. CPOC−H_2 organic cage (32.0 mg, 0.01 mmol) was dissolved in a mixed solvent of chloroform (60 mL) and methanol (20 mL), then the nickel acetate (35.4 mg, 0.2 mmol) was added in this reactor, the solution was stirred at room temperature for overnight, then washed with several portions of methanol, and dried over Na_2SO_4. Evaporation of the solvent gave 27.1 mg of a maroon solid with 81.7% yield. The progress of the reaction was monitored by Uv-vis spectrum. MALDI-TOF (m/z): $[M]^+$ 3261.0, found 3261.9.

Synthesis of CPOC−Cu. CPOC−H_2 organic cage (32.0 mg, 0.01 mmol) was dissolved in a mixed solvent of chloroform (60 mL) and methanol (20 mL), then the copper acetate (37.2 mg, 0.2 mmol) was added in this reactor, the solution was stirred at room temperature for overnight, then washed with several portions of methanol, and dried over Na_2SO_4. Evaporation of the solvent gave 26.0 mg of a dark brown solid with 80.8% yield. The progress of the reaction was monitored by Uv-vis spectrum. MALDI-TOF (m/z): $[M+2H]^+$ 3273.0, found 3272.7.

Synthesis of CPOC−Zn. CPOC−H_2 organic cage (32.0 mg, 0.01 mmol) was dissolved in a mixed solvent of chloroform (60 mL) and methanol (20 mL), then the zinc acetate (36.7 mg, 0.2 mmol) was added in this reactor, the solution was stirred at room temperature for overnight, then washed with several portions of methanol, and dried over Na_2SO_4. Evaporation of the solvent gave 28.1 mg of a dark green solid with 85.1% yield. The progress of the reaction was monitored by Uv-vis spectrum. MALDI-TOF (m/z): $[M+2H]^+$ 3275.0, found 3275.9.

Synthesis of CNDI. *N*,*N*'−bis(cyclohexyl)naphthalene diimide (CNDI) was synthesized following the previous literature. [S3]

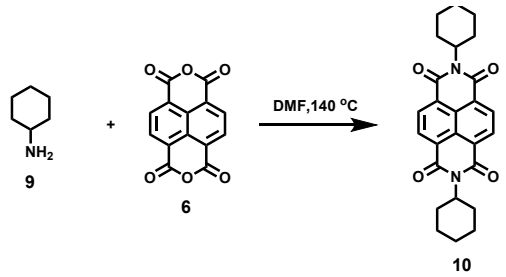

Scheme S3. Schematic synthesis of *N*,*N*'−bis(cyclohexyl)naphthalene diimide (**10**).

Synthesis of CNDI (10). A mixture of **6** (1.41 g, 5.26 mmol) and cyclohexylamine (1.29 g, 13.01 mmol) in DMF (25 mL) was heated under 140°C for 17 hours. The solvent was removed under reduced pressure. The residue was dry-loaded on silica and purified by column chromatography on silica using chloroform as eluent

to afford the pure product (2.06 g, 91.24%) as a yellowish to grey-yellowish solid. ^{1}H NMR (400 MHz, $CDCl_3$) δ 8.70 (s, 4H), 5.01 (tt, 2H), 2.65 – 2.40 (m, 4H), 1.91 (d, 4H), 1.82 – 1.68 (m, 6H), 1.53 – 1.21 (m, 6H).

Carbon Dioxide Electrocatalytic Reduction Measurement. Before the fabrication of electrode, a vial containing CPOC−Co (10.0 mg) or TPP−Co (4.8 mg), single−walled carbon nanotubes (CNTs) (30.0 mg), a Nafion perfluorinated resin solution (Sigma−Aldrich, 30 μL, 10 wt%), and THF (1.0 mL) was sonicated for 30 min to prepare a homogeneous paste. It is worthnoting that the mixture of catalyst and CNTs was ground prior to sonication. The electrode was fabricated by evenly transferring the paste (100.0 μL) with micro pipette on a carbon fiber paper (1.0 × 1.0 cm^2, TGP−H−60), making sure the CPOC−Co loading density of 1.0 mg cm^{-2} and TPP−Co loading density of 0.48 mg cm^{-2}. The paper electrode was dried at room temperature overnight. The experiments for CO_2 electrochemical reduction were conducted in a H−type electrochemical cell consisting of two compartments seperated by an anion exchange membrance (Nafion−117) on the electrochemical instrument (CHI760E) at 25°C in air−condition room. Two compartments containing 50.0 mL electrolyte (0.5 M $KHCO_3$ aqueous solution) with Pt foil and Ag/AgCl electrode in the saturated KCl solution as counter electrode and reference electrode, respectively. Prior to the electrochemical measurements, the electrolyte solution was saturated with Ar and CO_2 for 30 min. Linear sweep voltammetry (LSV) was operated with a scan rate of 10 mV s^{-1} from 0 to −1.63 V *vs*. Ag/AgCl in the CO_2 saturated 0.5 M $KHCO_3$ electrolyte (pH = 7.3). In this work, all mentioned potentials were converted to a RHE scale according to the equation of E (V *vs.* RHE) = E (*vs*. Ag/AgCl) + 0.059 × pH + 0.197. Electrical impedance spectroscopy of electrodes were tested in a CO_2-saturated $KHCO_3$ solution at a biased voltage of −0.4 V (vs RHE) with 5 mV amplitude in a frequency range from 100 kHz to 100 mHz. During the measurement, CO_2 gas at a flow rate of 20 mL min^{-1} was transported into the cell, and the product was analyzed by an online gas chromatograph (GC) (Shimadzu, Nexis GC-2030) equipped with a BID detector, the sampling loop (1.0 mL), and a CARBOH-ST column (30 m × 0 25 nm ID), Inlet temperature: 150 °C, Inlet pressure: 258 kPa, Column flow: 5 mL min^{-1}, linear velocity: 70 cm s^{-1}, Shunt ratio: 2.0, Total flow: 18 mL min^{-1}, Purge flow: 3 mL min^{-1}, Column temperature: 40 °C, BID1 temperature: 280 °C, BID1 Discharge electrical flow: 80 mL min^{-1}, Carrier gas: He. The peak areas were converted to gas concentration based on calibration curves. The liquid products were analyzed through nuclear magnetic resonance, in which 0.5 mL electrolyte was mixed with 100 μL of D_2O.

Calculation of Faradaic efficiency. The FE_X values of H_2 and CO were calculated on the basis of the equation I~III by using the concentrations (ppm) detected by the gas chromatograph as follows:

$$j_X = \frac{C \times v \times N \times F \times P_0}{R \times T \times S} \quad (\mathbf{I})$$

$$v_X = \frac{C \times v \times P_0}{R \times T \times S} \quad (\mathbf{II})$$

$$FE_X = \frac{j_X}{j_{Total}} \times 100\% = \frac{v_X \times N \times F}{j_{Total}} \times 100\% = \frac{C \times v \times N \times F \times P_0}{R \times T \times S \times j_{Total}} \times 100\% \quad (\mathbf{III})$$

For these equations, j_X and v_X are partial current density and production rate for a given gas product (CO or H_2), respectively. j_{Total} is the total current density. C is the concentration of the given gas product (CO or

H_2, ppm) detected by the gas chromatograph. *v* is CO_2 flow rate = 20 mL min^{-1} in this measurement. N = 2 is the number of electrons for CO_2-to-CO conversion. F is the Faraday constant of 96485 C mol^{-1}. P_0 is the atmospheric pressure 101.325 KPa, and R = 8.314 J mol^{-1} K^{-1} is the gas constant, T = 298.15 K and S is the electrode area (1.0 × 1.0 cm^2 in this measurement).

Calculation of Turnover Frequency (TOF, s^{-1}). The TOF for CO was calculated based on the following equations:

$$TOF = \frac{j_{total} \times FE_{CO}}{N \times F \times n_{total} \times f}$$

j_{total}: total current density; FE: Faradaic efficiency for CO production (%); N: the number of electrons transferred for product formation (here, it is 2for CO); F: Faradaic constant, 96485 C mol^{-1}; n_{total}: the total moles of catalyst employed in the electrolysis; *f*: the surface fraction of electrochemically active Co sites.

Calculation of turnover number (TON). TON is defined as the mole of reduction product generated per electrocatalytic active site over a given period. TON was calculated by the equation:

$$TON = \frac{Q \times FE(\%)}{N \times F \times n_{total} \times f}$$

Q: the total reduction charge pass during the electrolysis; FE: the estimated average CO faradaic efficiency during the electrolysis; N: the number of electron transferred for product formation (here, it is 2 for CO); F: Faradaic constant, 96485 C mol^{-1}; n_{total}: the total moles of catalyst employed in the electrolysis; *f*: the surface fraction of electrochemically active Co sites.

Cyclic Voltammograms (CV) measurement. Electrochemical measurements were carried out with a CHI760E electrochemical work station. The cell comprised inlets for a glassy−carbon−disk working electrode with a diameter of 2.0 mm in diameter and a platinum wire counter electrode. The reference electrode was Ag^+/Ag (a solution of 0.01 M $AgNO_3$ in acetonitrile), which was connected to the solution by a Luggin capillary whose tip was placed close to the working electrode. It was corrected for junction potentials by being referenced internally to the ferrocenium/ferrocene (Fc^+/Fc) couple [$E_{1/2}(Fc^+/Fc)$ = 0.501 V *vs.* SCE]. Typically, a 0.1 M solution of $[Bu_4N][ClO_4]$ (TBAP) in CH_2Cl_2 containing 3 mM of sample was purged with nitrogen for 15 min, and then the voltammograms were recorded at ambient temperature. The scan rate was 50 mV s^{-1} for the CV measurement.

Determination of surface concentration of electroactive cobalt porphyrin units in CPOC−Co and TPP-Co. To estimate the surface concentration of electroactive cobalt porphyrin units in CPOC−Co, cyclic voltammetry tests of CPOC−Co and TPP−Co in Ar saturated 0.5 M $KHCO_3$ were conducted. The CV curves were tested at 60, 80 and100 mV s^{-1}. We integrated the anodic wave in the CV curve of CPOC−Co and TPP−Co, and then calculated the amount of electrochemically active sites using the following equation: $\Gamma = Q_{CV}/nFA$, where Q_{CV} is the integration of the peak area under the Co(I)/Co(II) anodic wave, *n* is the number electrons transferred for the redox couple (*n* = 1), *F* is the Faraday constant, and *A* is the surface area of the electrode.[S4, S5]

Physical characterization. NMR spectra were recorded on a Bruker DPX 400 spectrometer (^{1}H: 400 MHz, ^{13}C: 100 MHz) in $CDCl_3$. ^{1}H NMR spectra were referenced internally using the residual solvent resonances (δ = 7.26 ppm for $CDCl_3$) relative to $SiMe_4$. Uv-vis absorption spectra were recorded on a Lambda 750 spectrophotometer. FT−IR spectra were recorded as KBr pellets using a Bruker Tensor 37 spectrometer with 2 cm^{-1} resolution. MALDI−TOF mass spectra were taken on a Bruker BIFLEX III ultra−high resolution Fourier transform ion cyclotron resonance (FT−ICR) mass spectrometer, aquisition operation mode: Reflector; voltage polarity: POS; number of shots: 2000; the matrix component: α-Cyano-4-hydroxycinnamic acid. X−ray photoelectron spectroscopy (XPS) data were conducted on an ESCALAB 250Xi system. Al Kα X−ray (6 mA × 12 KV) was utilized as the irradiation source. All measurements were performed in the CAE mode with the reference of C 1s (284.8 eV). The CO_2 adsorption and desorption isotherms were measured at 298 and 273 K using a Micromeritics ASAP 2020 PLUS HD88 system. The samples were degassed at 60°C for 10 hours before the measurement. The Co content of the CPOC−Co was determined by inductively coupled plasma (ICP) analysis with an Aglient 725−ES ICP−MS instrument. The transmission electron microscopy (TEM) was acquired on HITACHI HT7700 with an electron acceleration energy of 100 kV.

TA experiment. The pump beam was generated from a regenerative amplified Ti: sapphire laser system from Coherent (800 nm, 100 fs, 6 mJ per pulse, and 1 kHz repetition rate). The 800 nm output pulse from the regenerative amplifier was split into two parts with a beam splitter. The reflected part was used to pump a TOPAS Optical Parametric Amplifier (OPA) which generates a wavelength-tunable laser pulse from 250 nm to 2.5 mm as the pump beam. The transmitted 800 nm beam was attenuated with a neutral density filter and focused into a rotating CaF_2 disk to generate a white light continuum (WLC) from 350 to 800 nm used for the probe beam. The probe beam was focused with an Al parabolic reflector onto the sample. After the sample, the probe beam was collimated and then focused into a fiber-coupled spectrometer and detected at a frequency of 1 kHz. The intensity of the pump pulse used in the experiment was controlled by a variable neutral-density filter wheel. The delay between the pump and probe pulses was controlled by a motorized delay stage. The pump pulses were chopped by a synchronized chopper at 500 Hz.

Computational methods. The solvent effects of water media have been taken into account via the self−consistent reaction field (SCRF) method, using the SMD solvent model. And the PBE0 functional was performed in the selected fragment calculations through the Gaussian09 program [S6, S7]. The 6−31G(d) basis [S8-S10] was chosen for C, H, O, N atoms, and SDD basis [S11] was chosen for metal atoms. The dispersion correction has been considered by using D3BJ [S12] and the Natural population analysis (NPA) charge was presented. The Mayer bond order was analyzed by the Multiwfn package[S13-S15]. As shown in Fig. 4b, the selected fragment was consisting of metal−porphyrin unit.

Results and Discussion

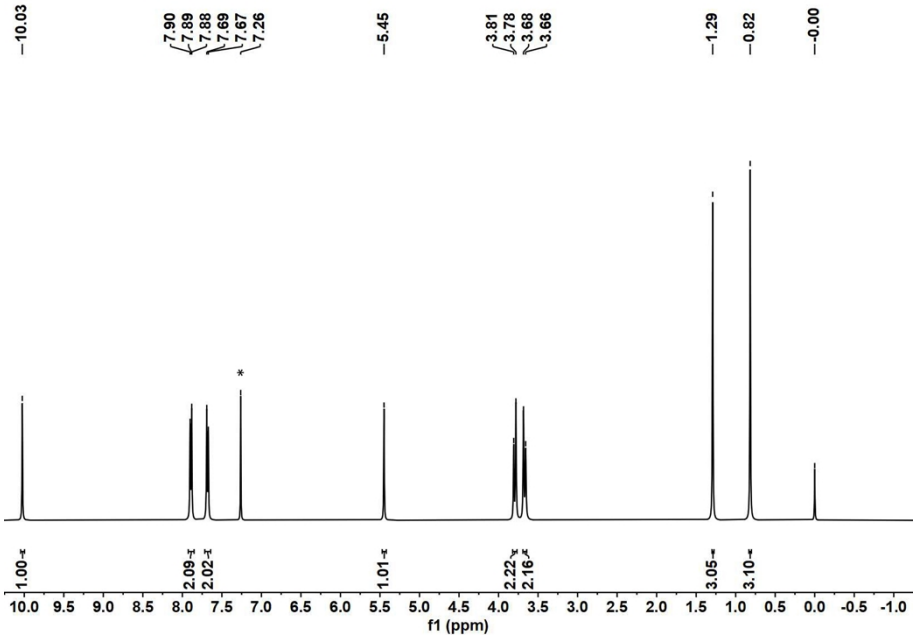

Fig. S1 ^{1}H NMR spectrum of 4−(5,5−dimethyl−1,3−dioxan−2−yl)benzaldehyde (2) in $CDCl_3$. (* denotes $CDCl_3$ solvent impurity at 7.26)

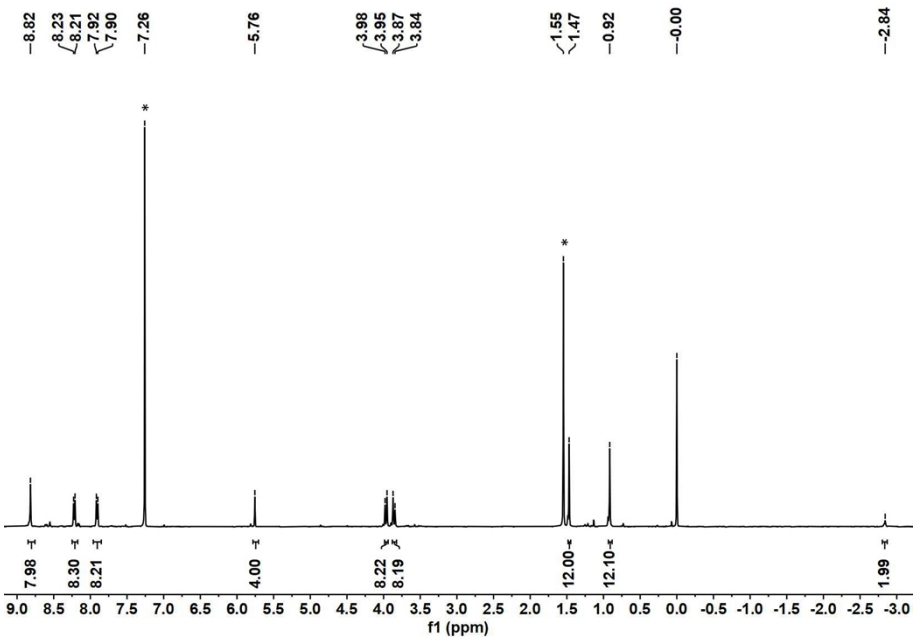

Fig. S2 ^{1}H NMR spectrum of tetrakis[4−(1,3−dioxa−5,5−dimethylcyclohex−2−yl)phenyl]porphyrin (3) in $CDCl_3$. (* denotes $CDCl_3$ solvent impurity at 7.26, and the peak at 1.55 attributes to H_2O.)

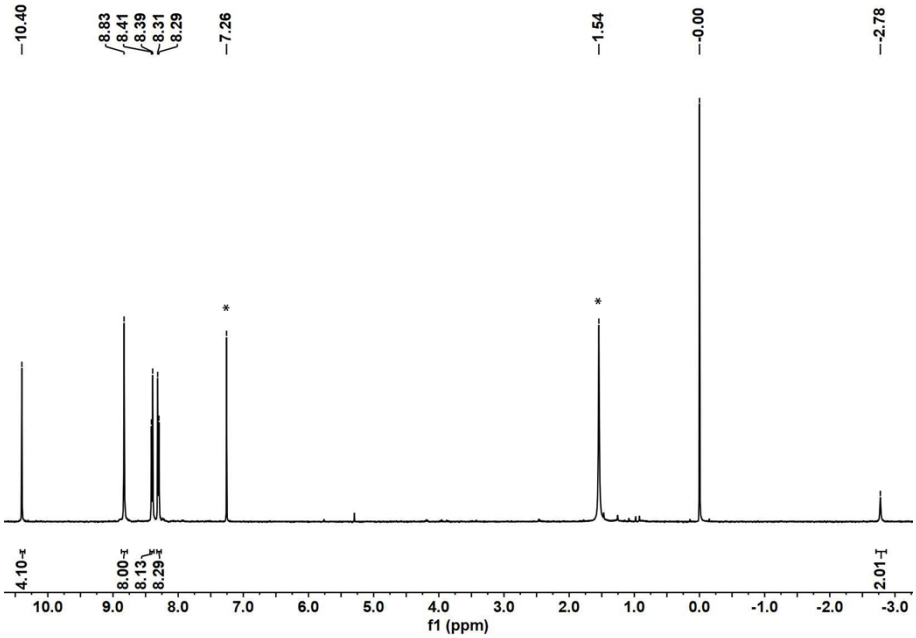

Fig. S3 ^{1}H NMR spectrum of *meso*−tetra(p−formylphenyl)porphyrin (4) in $CDCl_3$. (* denotes $CDCl_3$ solvent impurity at 7.26, and the peak at 1.54 attributes to H_2O.)

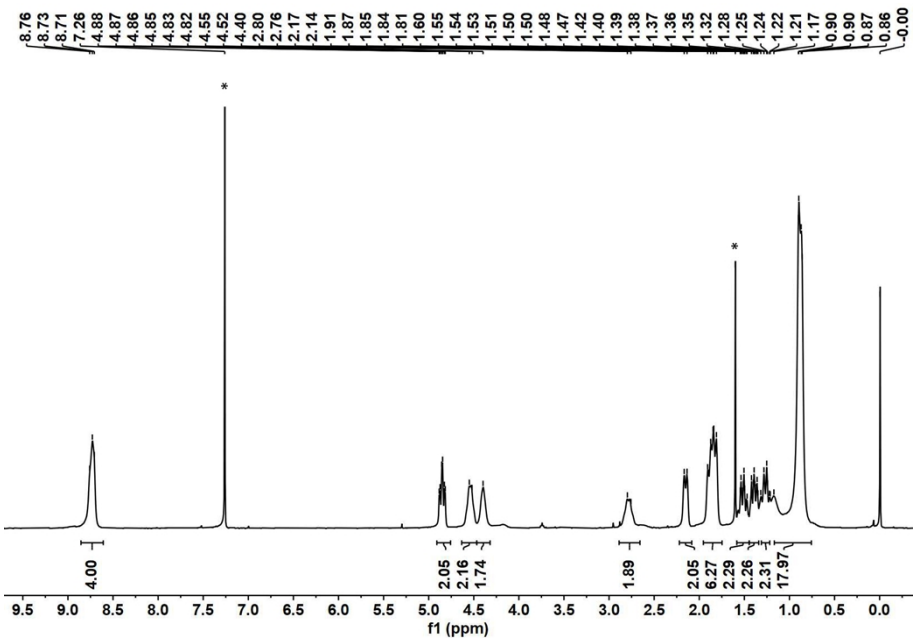

Fig. S4 ^{1}H NMR spectrum of protected NDI diamine (7) in $CDCl_3$. (* denotes $CDCl_3$ solvent impurity at 7.26, and the peak at 1.56 attributes to H_2O.)

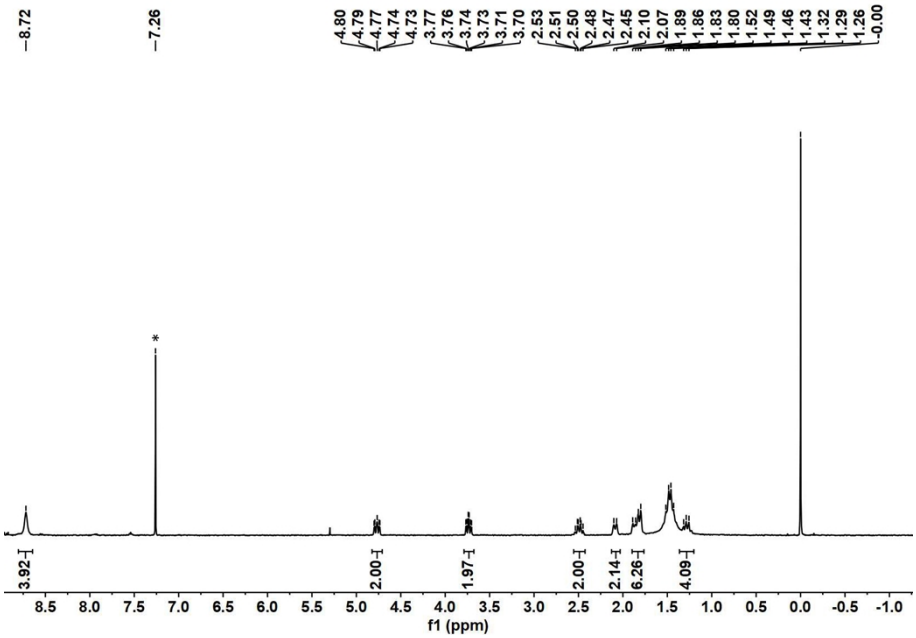

Fig. S5 ^{1}H NMR spectrum of ANDI (8) in $CDCl_3$. (* denotes $CDCl_3$ solvent impurity at 7.26)

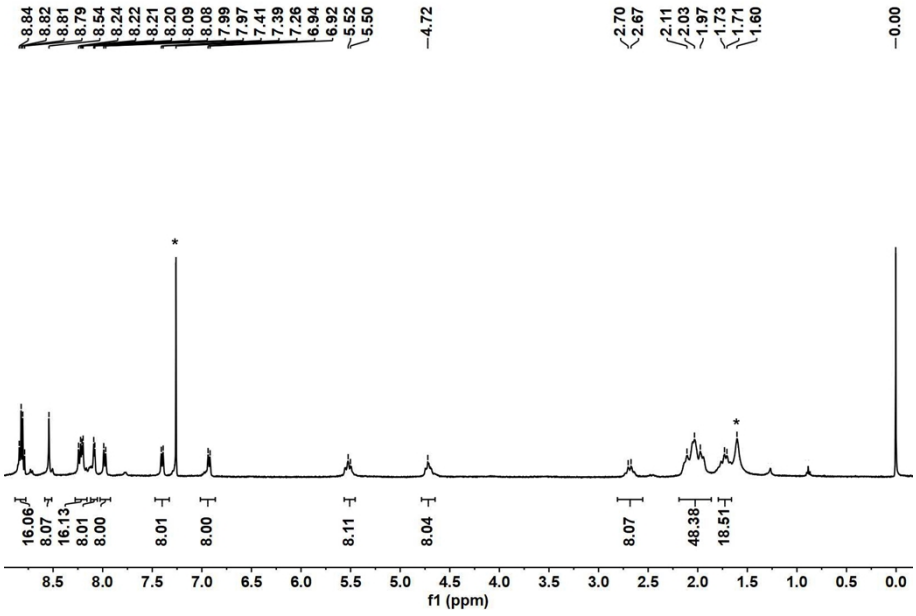

Fig. S6 ^{1}H NMR spectrum of CPOC-H_2 in $CDCl_3$. (* denotes $CDCl_3$ solvent impurity at 7.26, and the peak at 1.60 attributes to H_2O.)

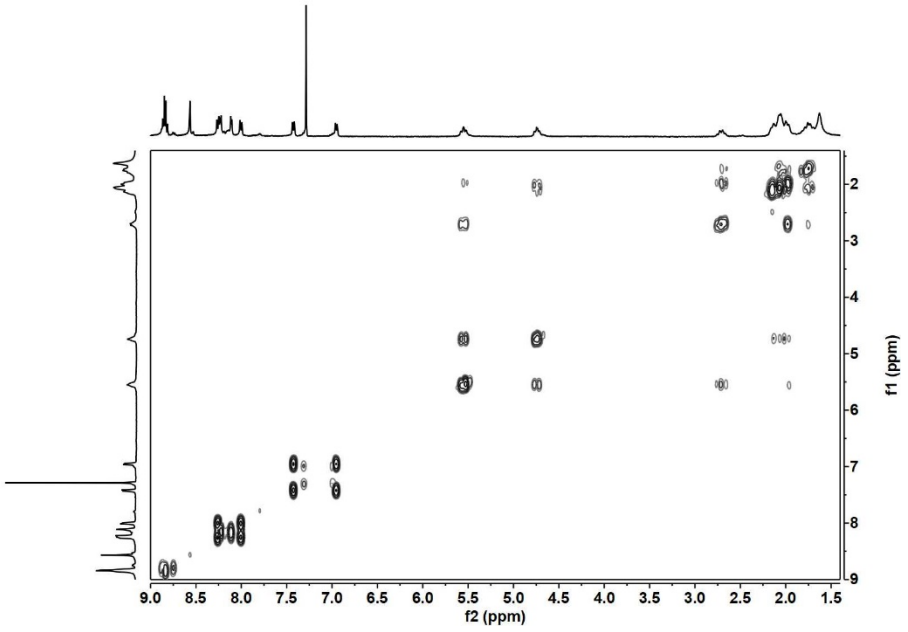

Fig. S7 $^{1}H-^{1}H$ COSY spectrum of CPOC−H_2 recorded in $CDCl_3$.

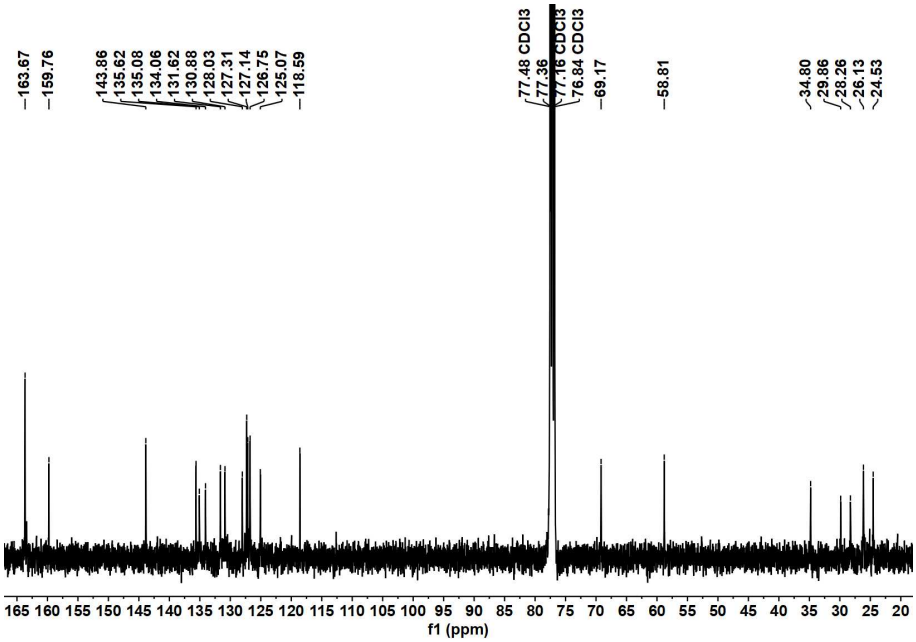

Fig. S8 ^{13}C NMR spectrum of CPOC−H_2 recorded in $CDCl_3$.

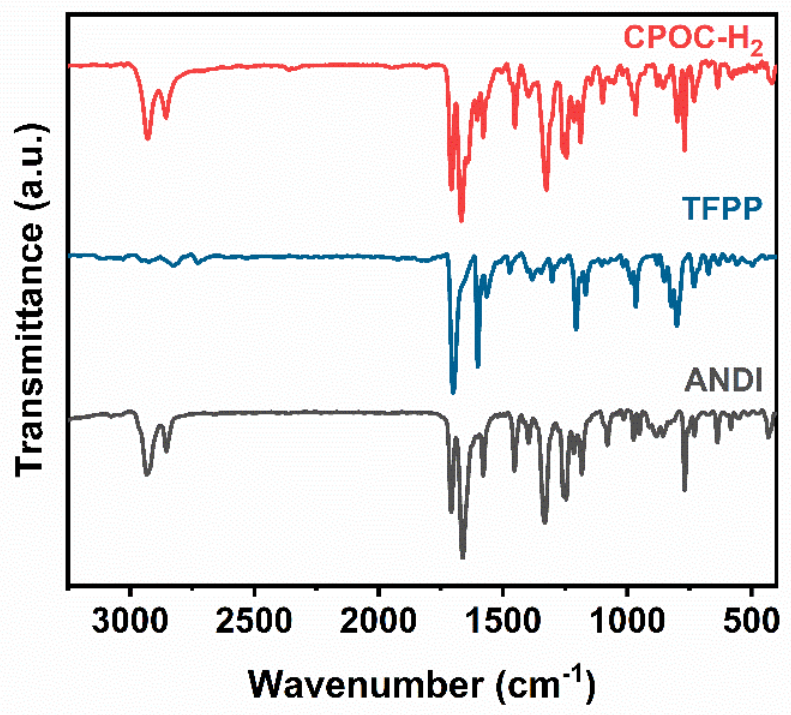

Fig. S9 FT−IR spectra of CPOC−H_2 and the corresponding monomer.

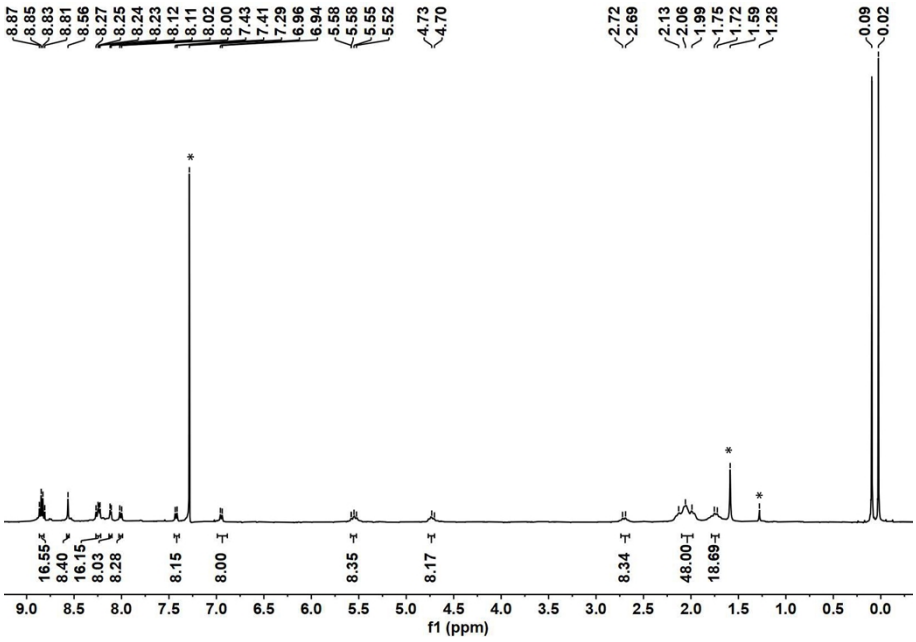

Fig. S10 ^{1}H NMR spectrum of CPOC-Zn in $CDCl_3$. (* denotes $CDCl_3$ solvent impurity at 7.26, the peak at 1.59 attributes to H_2O and the peak at 1.28 attributes to H grease.)

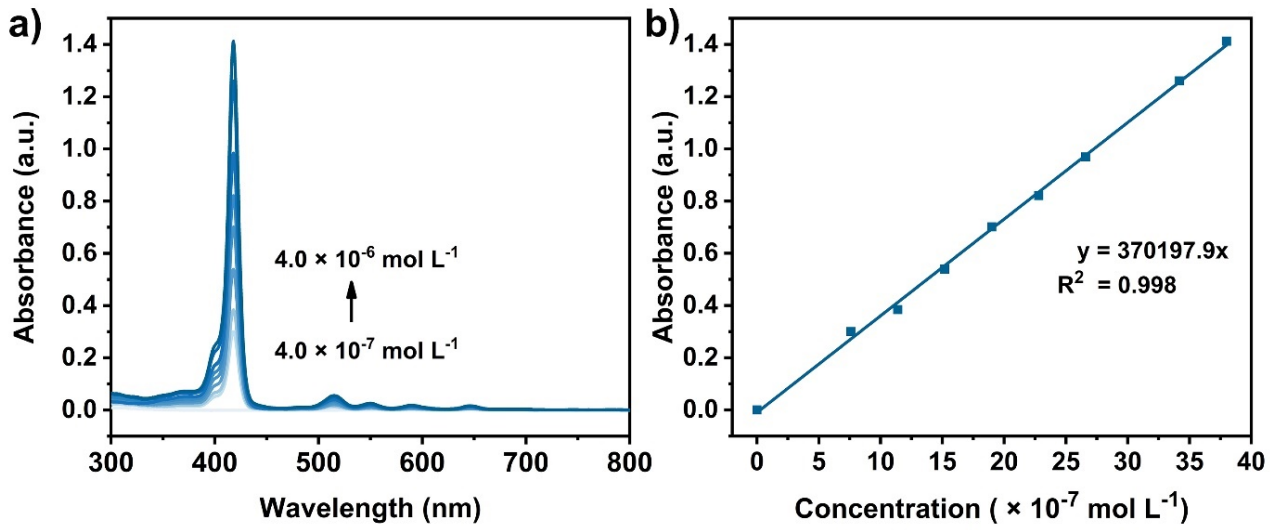

Fig. S11 (a) The absorption spectra of TPP in $CHCl_3$ and (b) corresponding BeerLambert plot recorded at maximium of 422 nm.

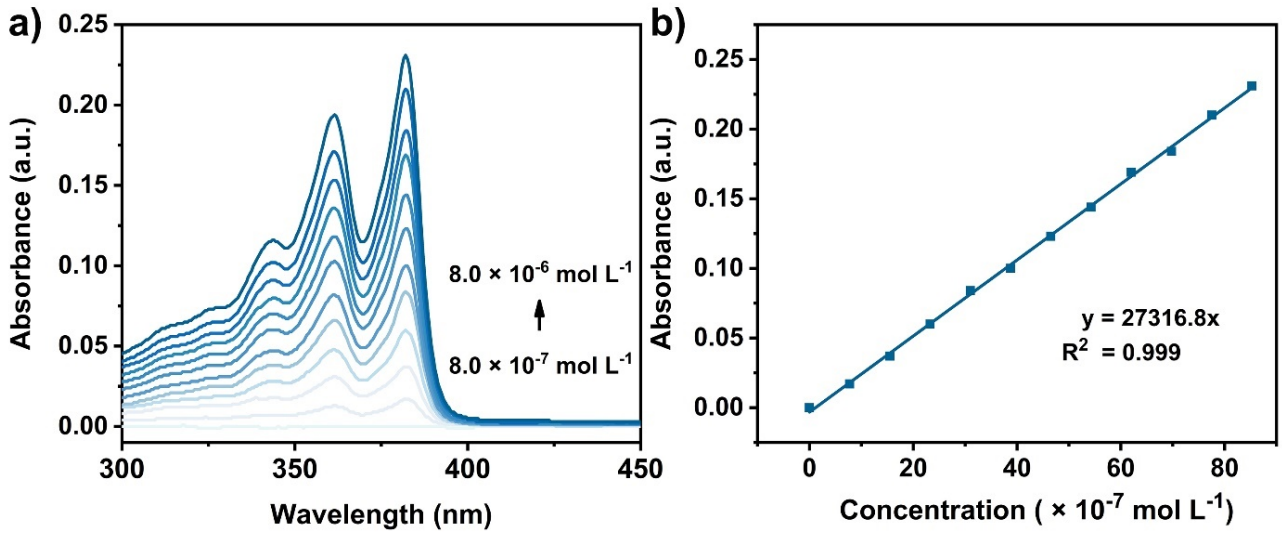

Fig. S12 (a) The absorption spectra of CNDI in $CHCl_3$ and (b) corresponding BeerLambert plot recorded at maximium of 383 nm.

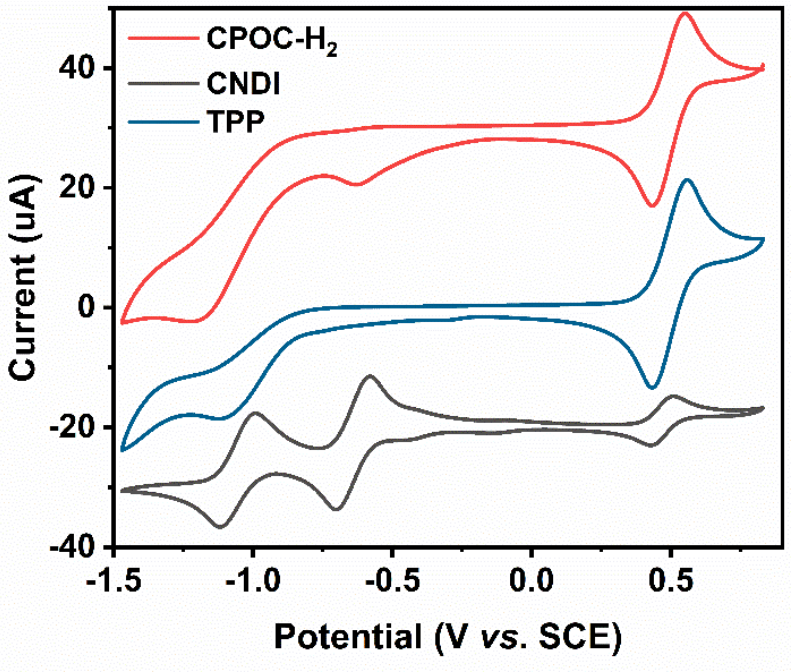

Fig. S13 Cyclic voltammograms of CPOC−H_2 and the corresponding monomeric references in CH_2Cl_2 containing 0.1 M TBAP at a scan rate of 50 mV s^{-1}.

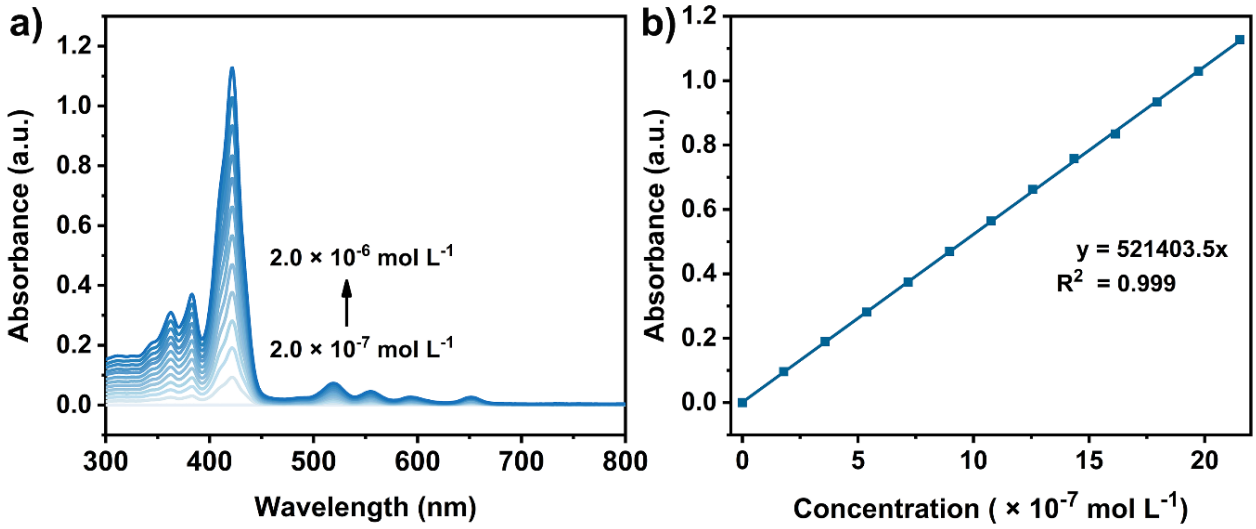

Fig. S14 (a) The absorption spectra of CPOC−H_2 in $CHCl_3$ and (b) corresponding BeerLambert plot recorded at maximium of 422 nm.

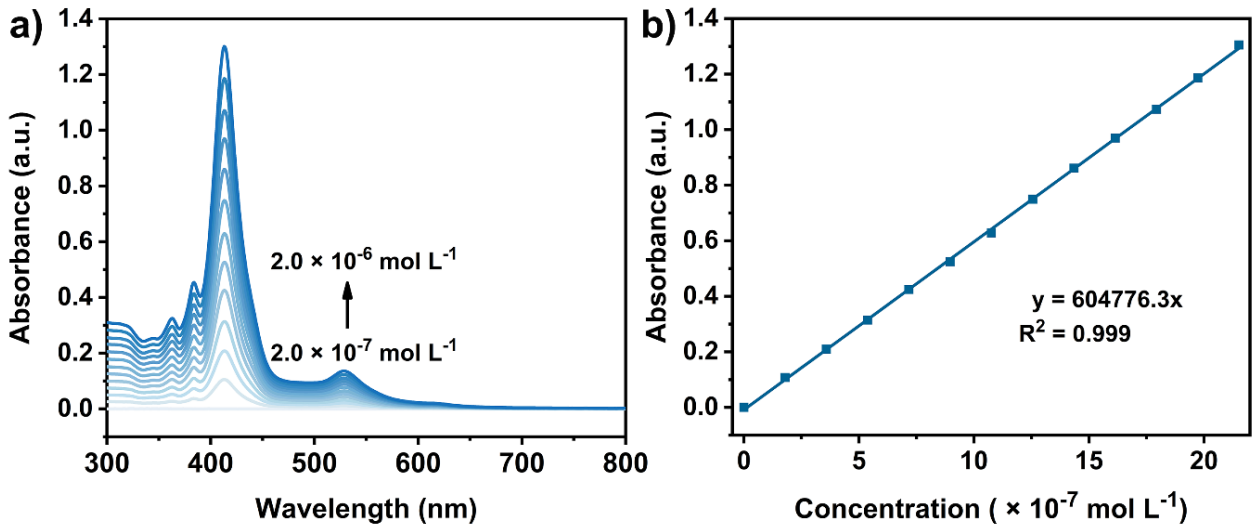

Fig. S15 (a) The absorption spectra of CPOC−Co in $CHCl_3$ (b) corresponding BeerLambert plot recorded at maximium of 422 nm.

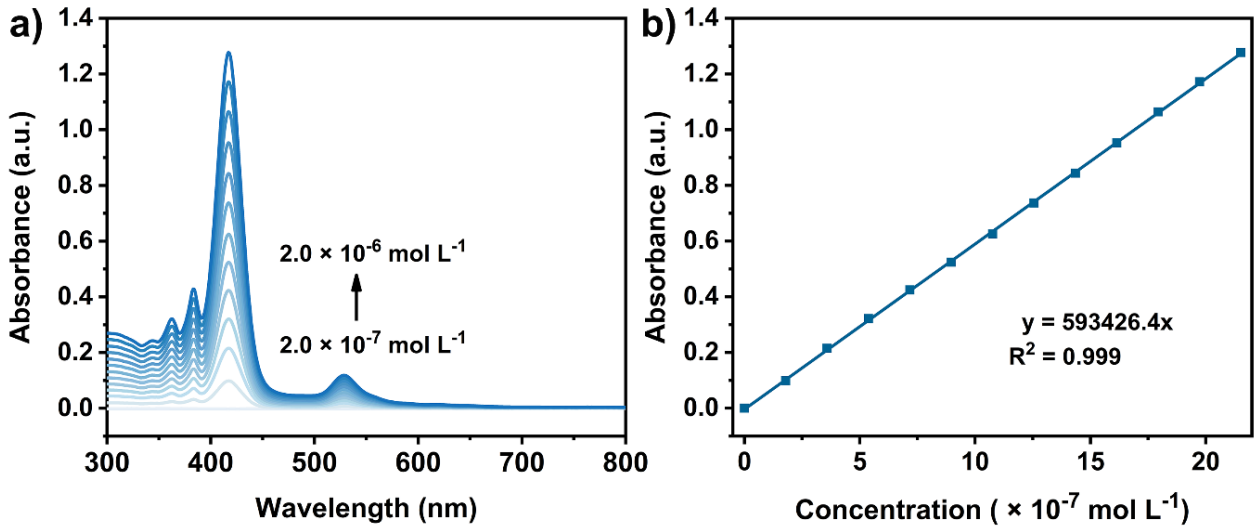

Fig. S16 (a) The absorption spectra of CPOC−Ni in $CHCl_3$ (b) corresponding BeerLambert plot recorded at maximium of 422 nm.

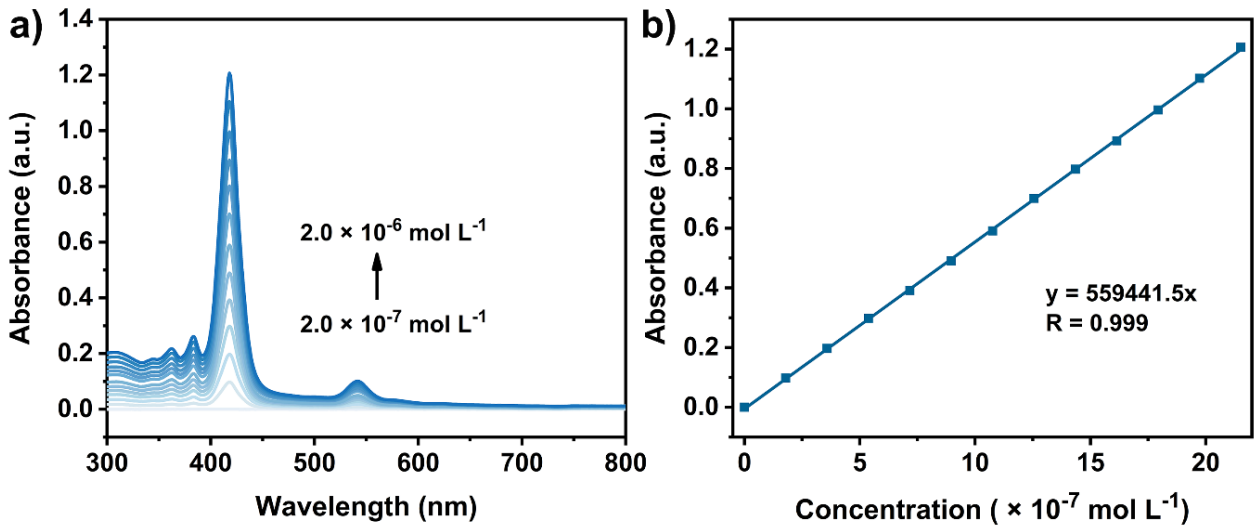

Fig. S17(a) The absorption spectra of CPOC−Cu in $CHCl_3$ (b) corresponding BeerLambert plot recorded at maximium of 422 nm.

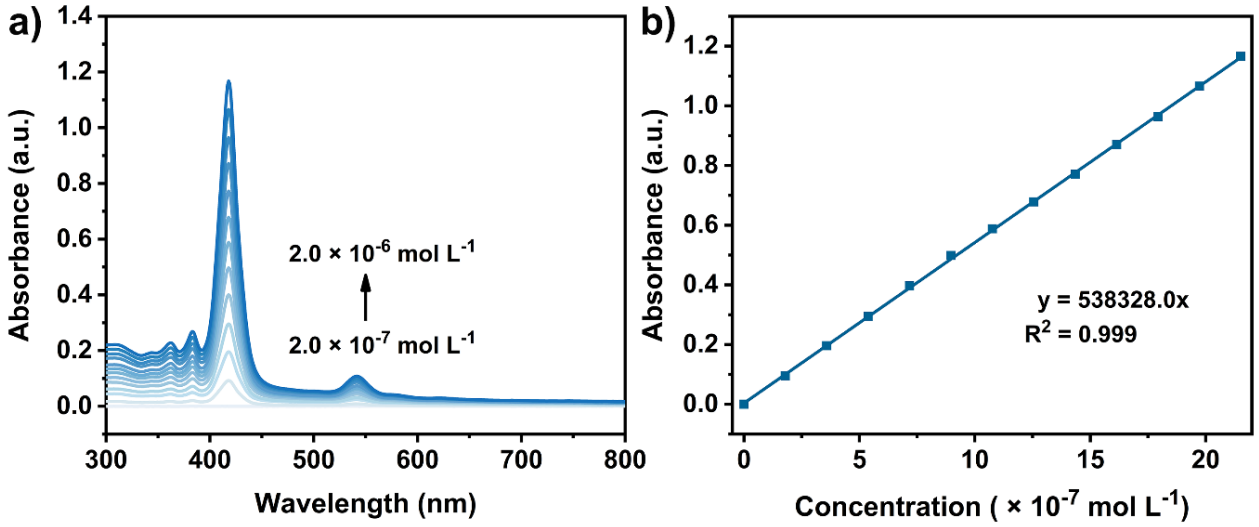

Fig. S18 (a) The absorption spectra of CPOC−Zn in $CHCl_3$ (b) corresponding BeerLambert plot recorded at maximium of 422 nm.

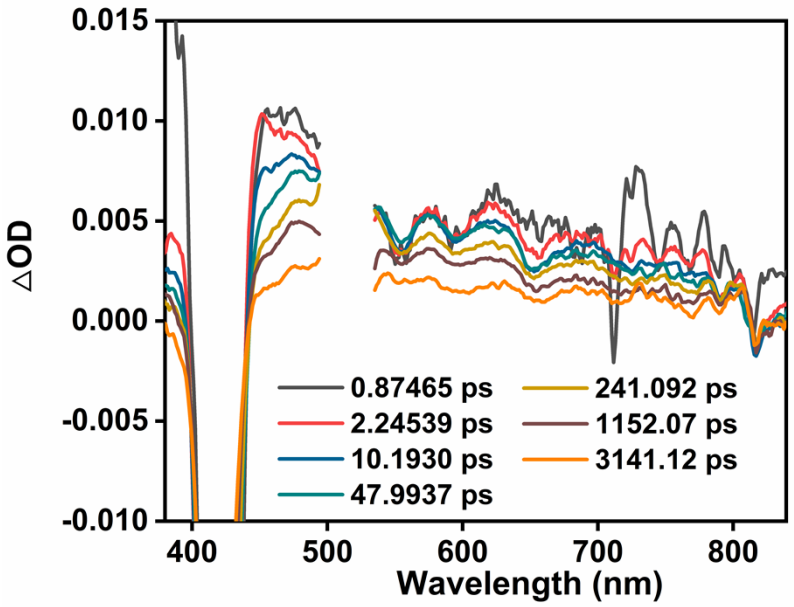

Fig. S19 The enlarged fs-TA spectra of CPOC-H_2.

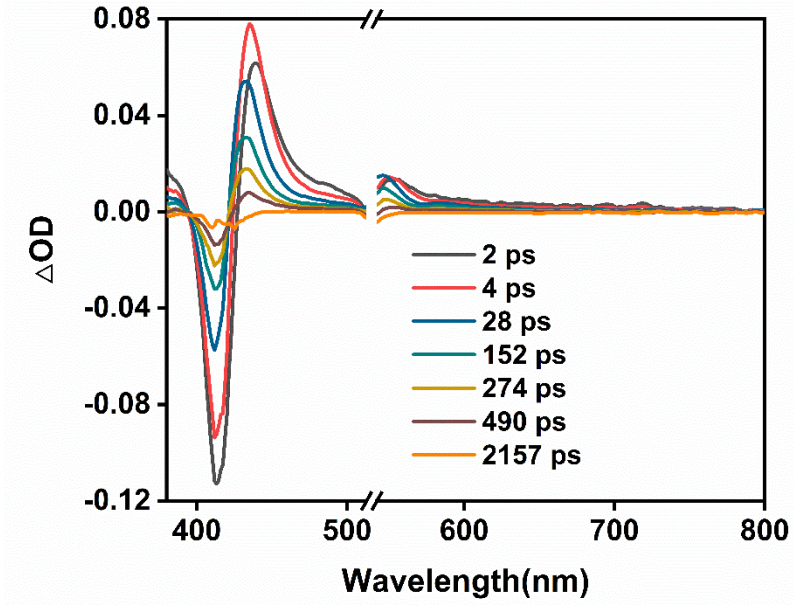

Fig. S20 TA of CPOC−Ni in degassed toluene excited at 530 nm.

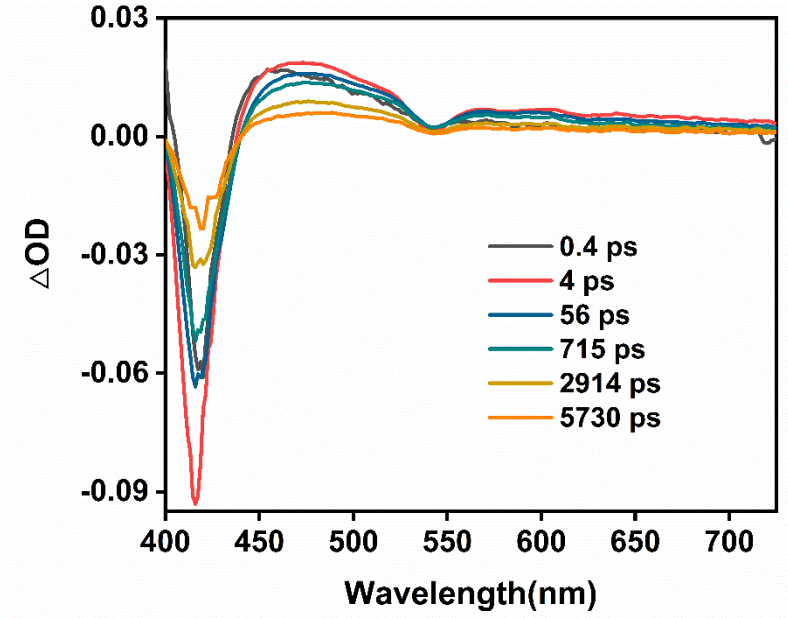

Fig. S21 TA of CPOC−Cu in degassed toluene excited at 540 nm.

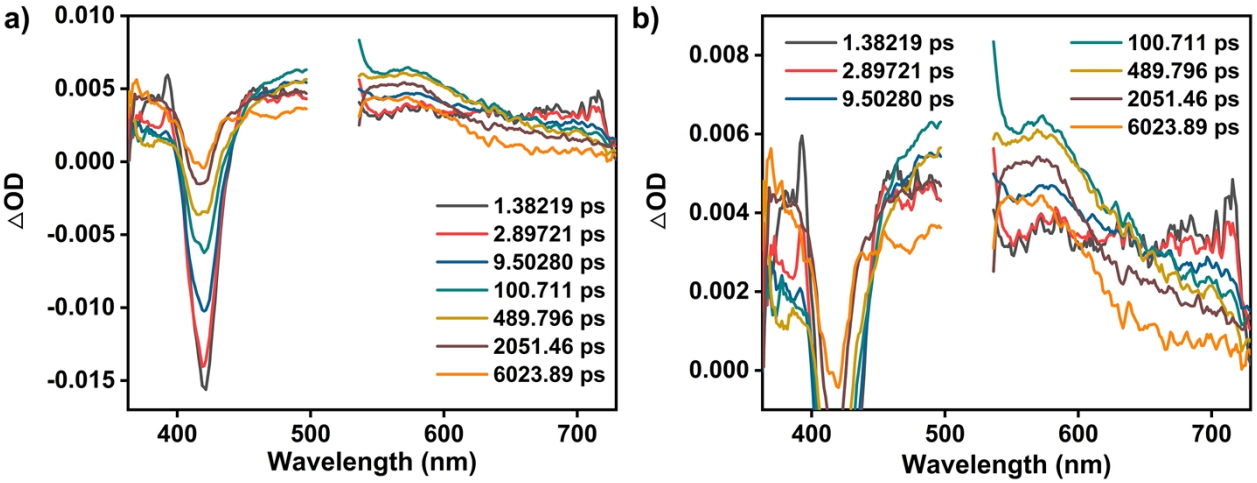

Fig. S22 (a) TA of CPOC−Zn in degassed toluene excited at 520 nm and (b) the enlarged fs-TA spectra of CPOC-Zn.

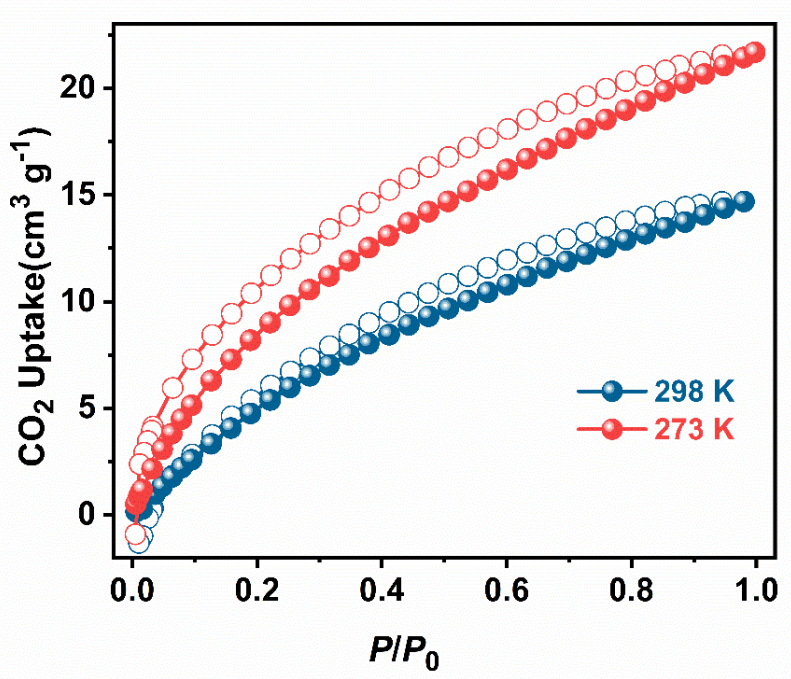

Fig. S23 CO_2 adsorption (solid) and desorption (hollow) curves at 298 K (black) and 273 K (red) of CPOC−Co.

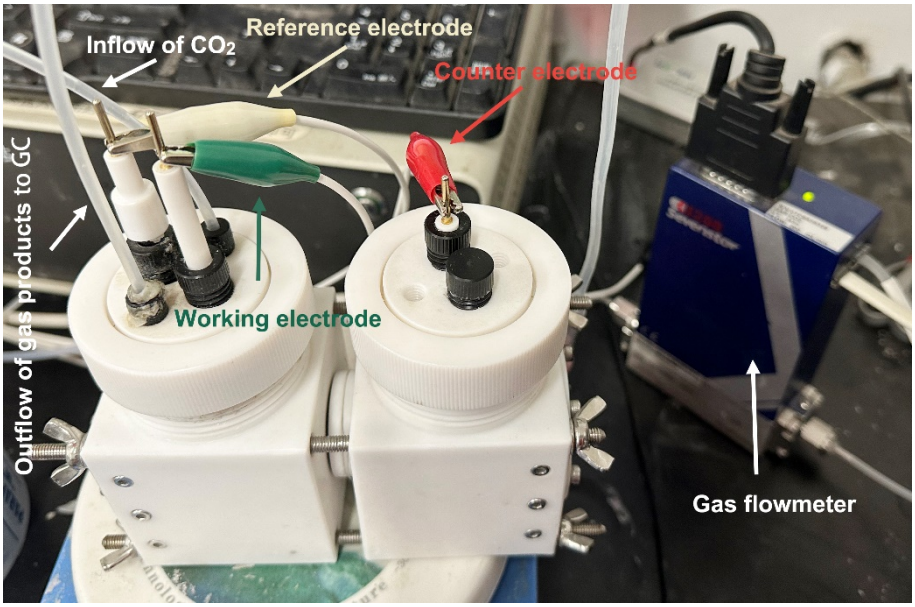

Fig. S24 Photograph of three-electrode H-type cell for the electrochemical CO_2RR measurements.

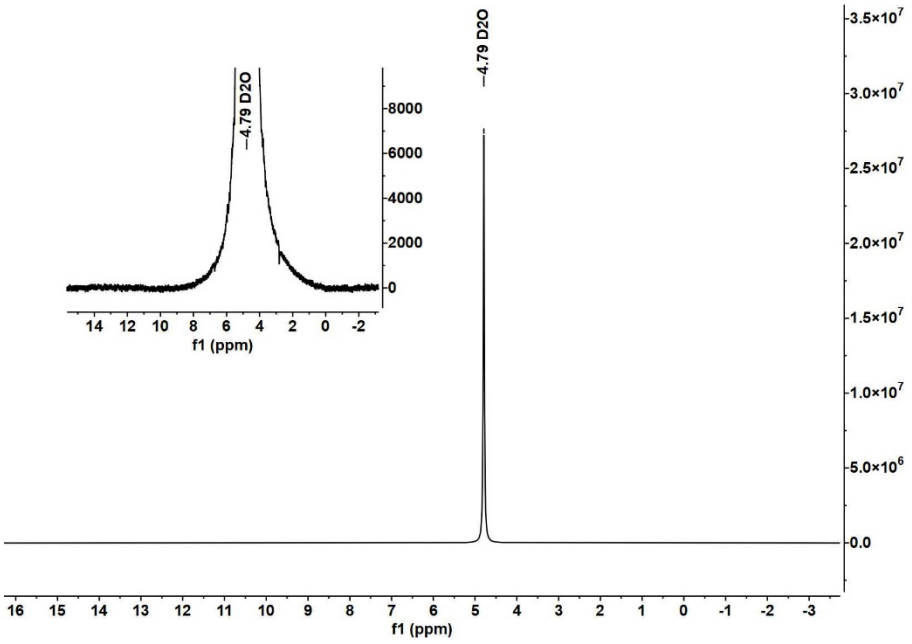

Fig. S25 ^{1}H NMR spectra of the electrolyte for CPOC−Co after continuous CO_2RR test at the potential from −0.40 to −0.90 V (*vs*. RHE) in D_2O.

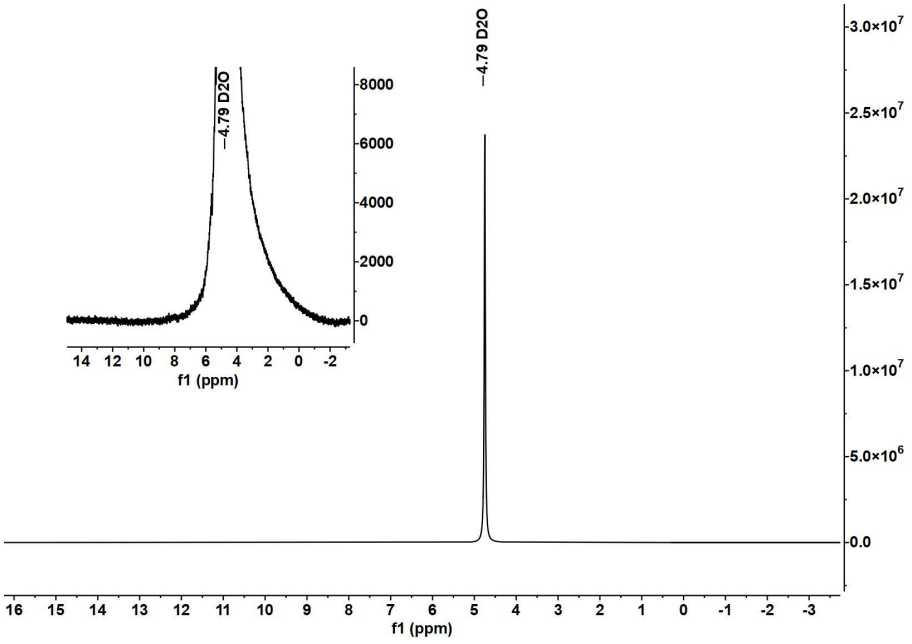

Fig. S26 ^{1}H NMR spectra of the electrolyte for TPP−Co after continuous CO_2RR test at the potential from −0.40 to −0.90 V (*vs*. RHE) in D_2O.

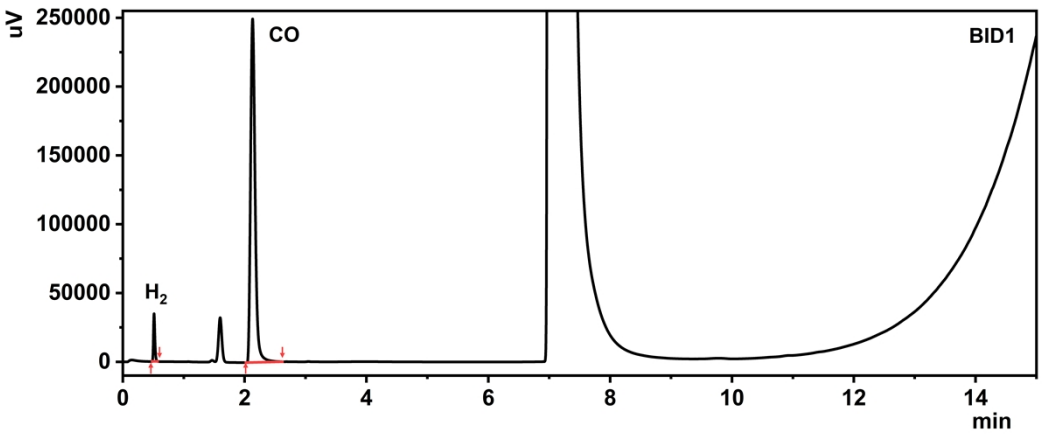

Fig. S27 GC plots of the gas products for CPOC−Co at -0.7 V (*vs*. RHE) in H-type cell.

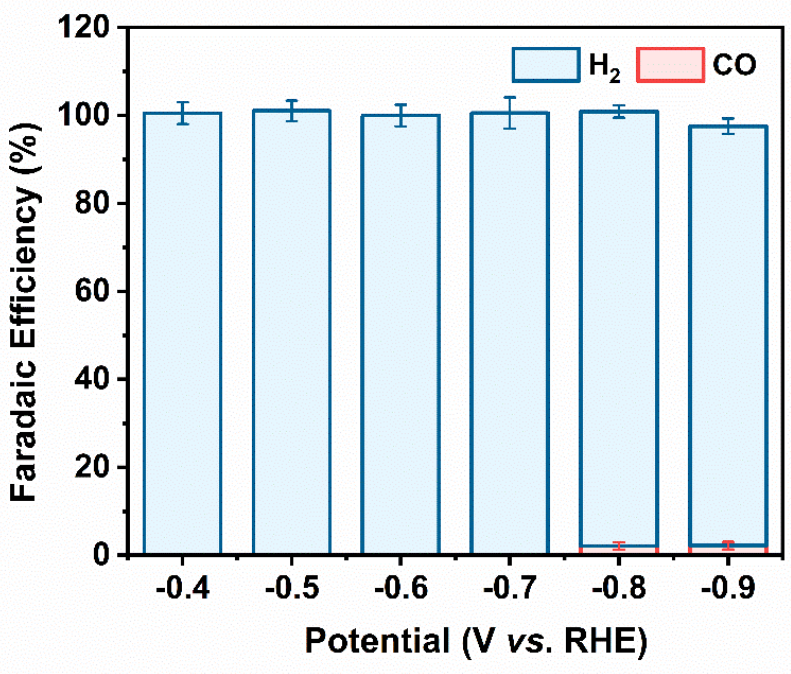

Fig. S28 FE_{CO} and FE_{H2} of CPOC−Co at different applied potentials in Ar saturated 0.5M $KHCO_3$ aqueous solution.

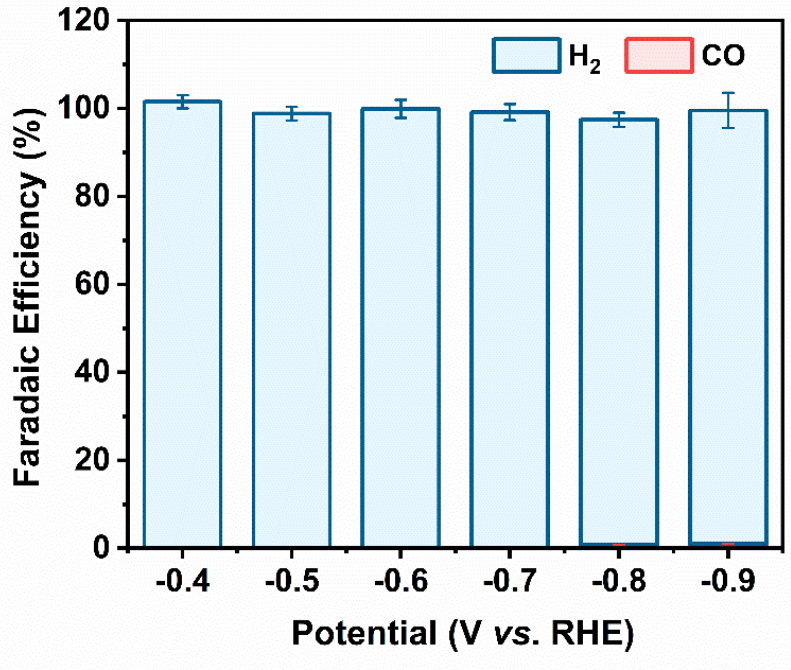

Fig. S29 FE_{CO} and FE_{H2} of the carbon cloth with CNTs and Nafion at different applied potentials in CO_2 saturated 0.5 M $KHCO_3$ aqueous solution.

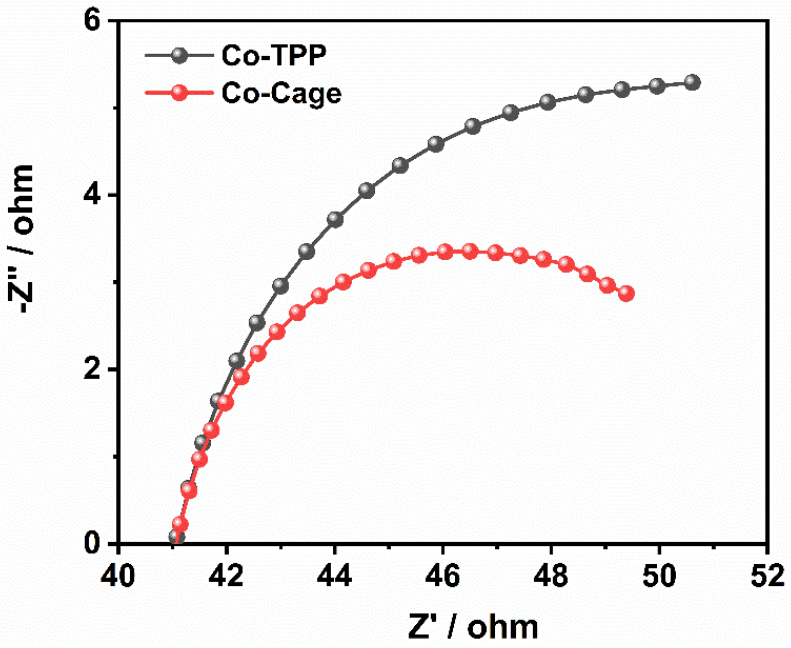

Fig. S30 EIS of CPOC−Co and TPP−Co.

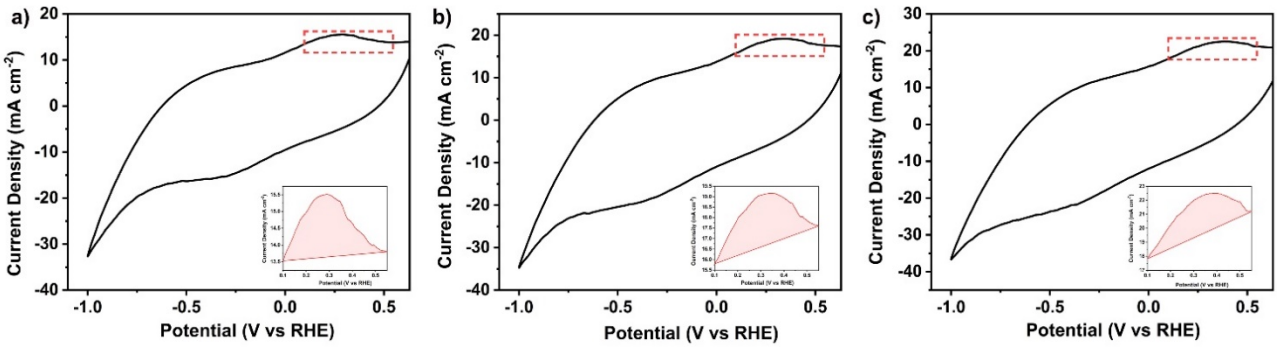

Fig. S31 Cyclic voltammetry curves of the CPOC−Co in Ar saturated 0.5 M $KHCO_3$ at scan rate of 60 (a), 80 (b), and 100 (c) mV s^{-1}. Insert shows the total charge integrated from the Co(I)/Co(II) anodic wave.

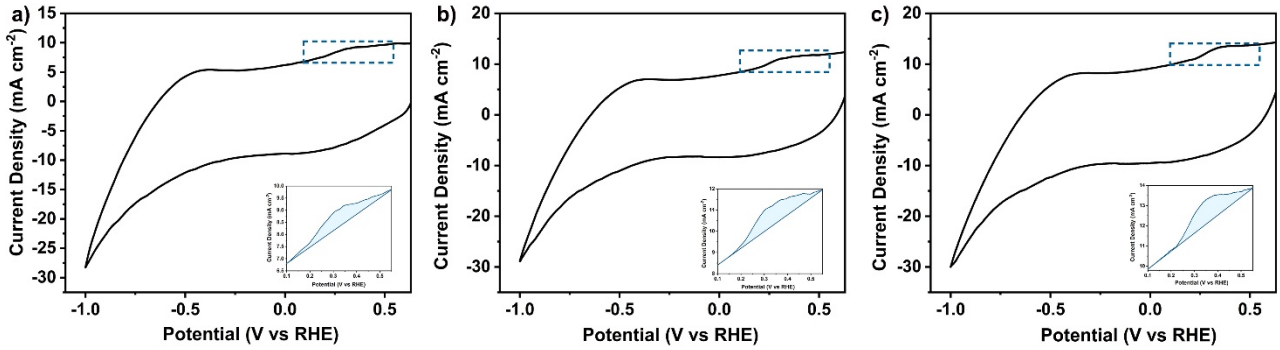

Fig. S32 Cyclic voltammetry curves of the TPP−Co in Ar saturated 0.5 M $KHCO_3$ at scan rate of 60 (a), 80 (b), and 100 (c) mV s^{-1}. Insert shows the total charge integrated from the Co(I)/Co(II) anodic wave.

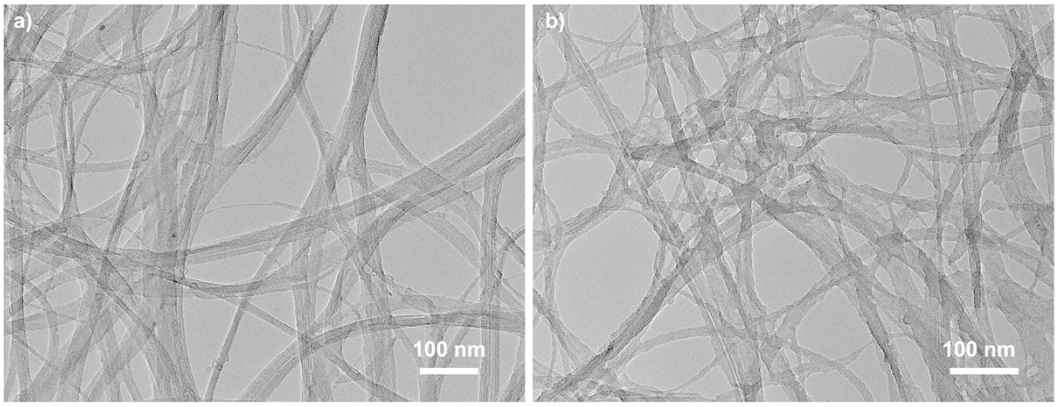

Fig. S33 TEM images of (a) CNT and (b) CPOC−Co@CNT.

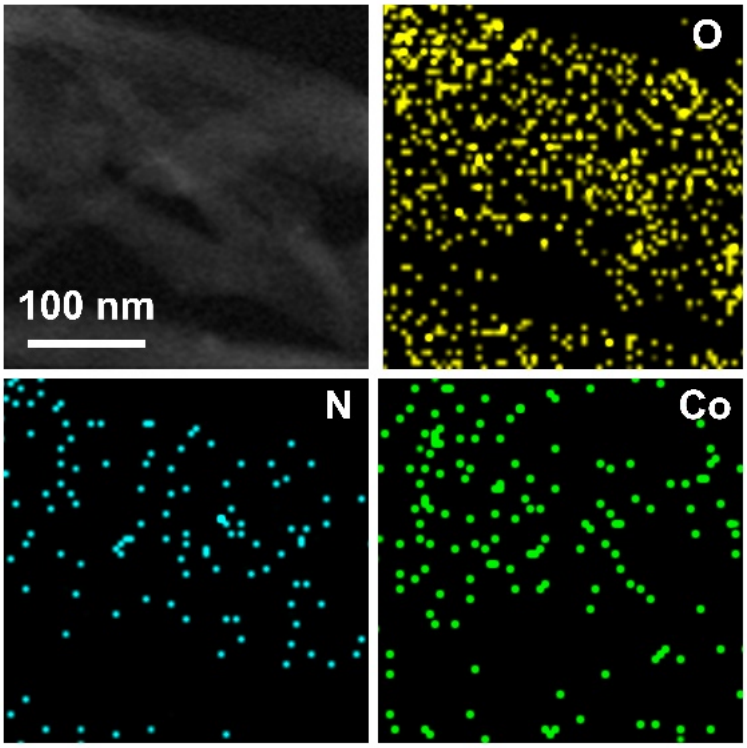

Fig. S34 Energy dispersive X-ray spectroscopy element mapping CPOC-Co@CNT.

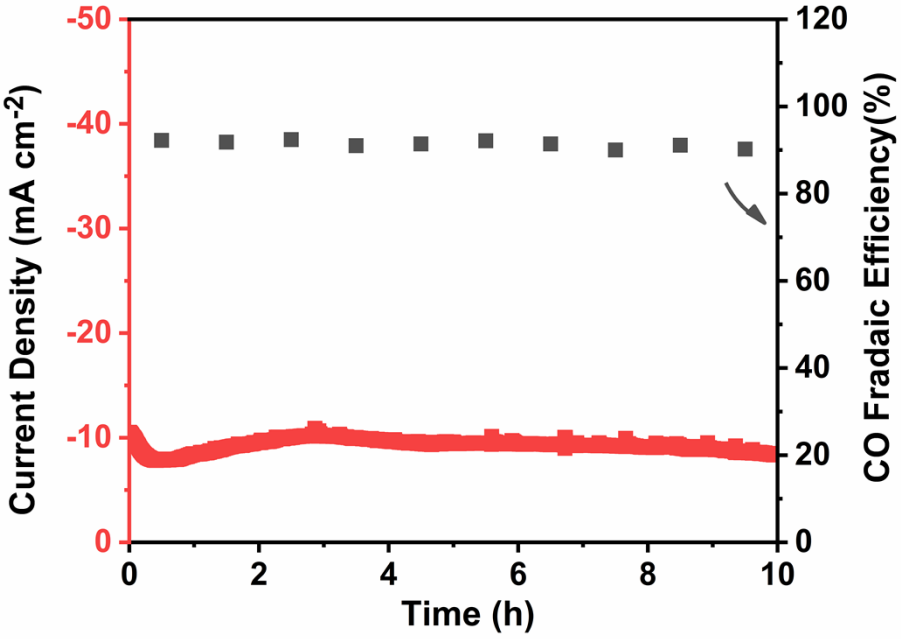

Fig. S35 Stability test at −0.70 V for 10 h about CPOC−Co.

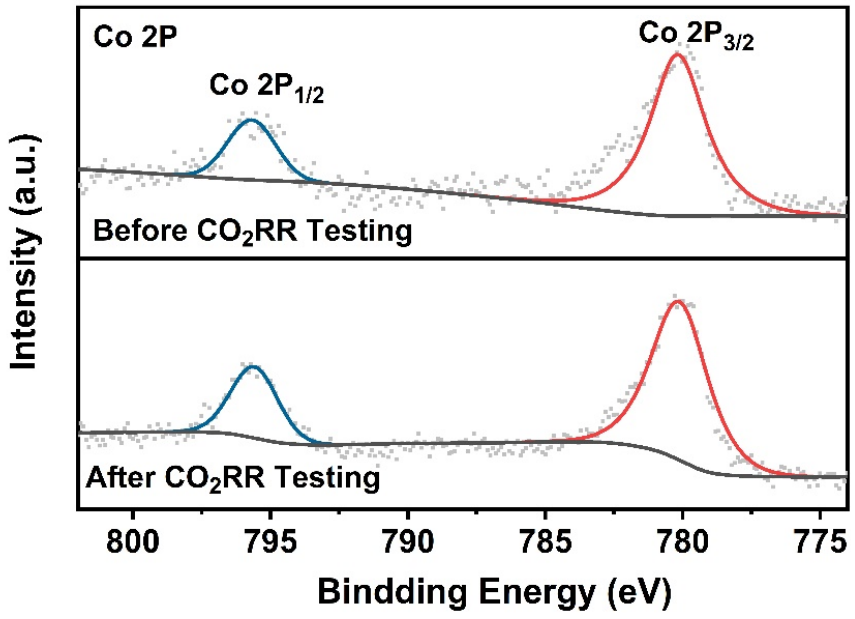

Fig. S36 High−resolution XPS spectra of CPOC−Co before and after CO_2RR testing.

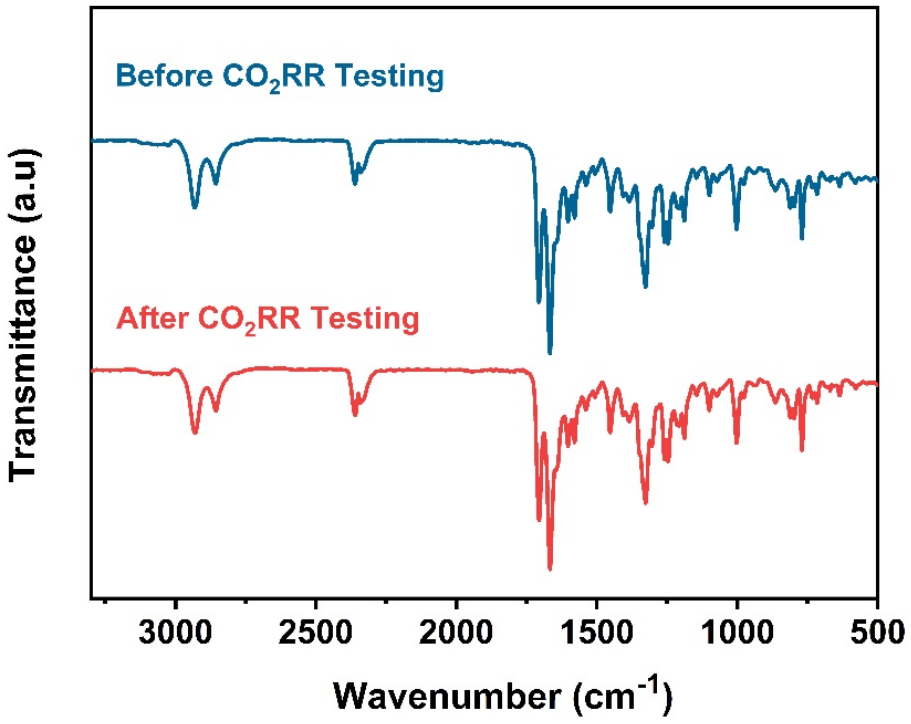

Fig. S37 FT−IR spectra of CPOC−Co before and after CO_2RR testing.

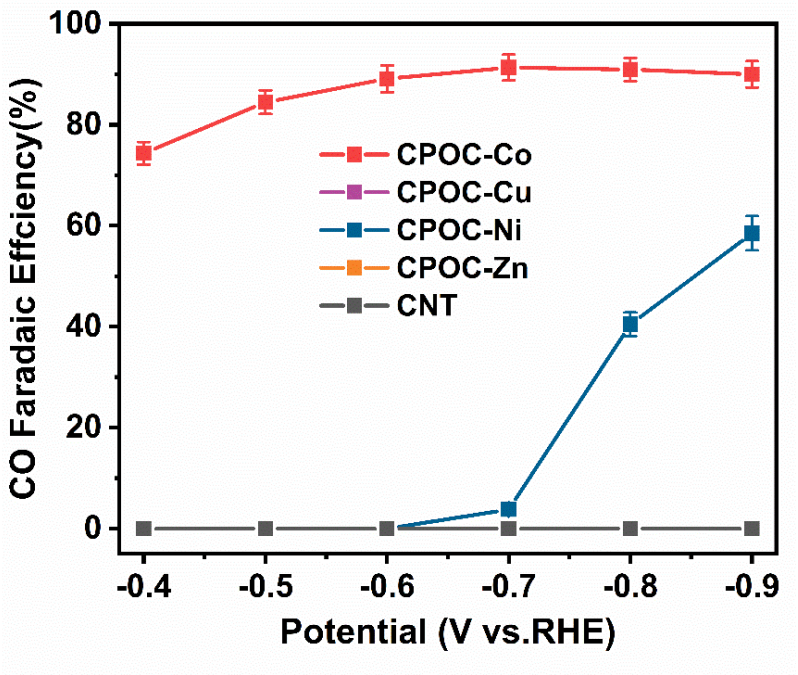

Fig. S38 Faradaic efficiency of CPOC−M.

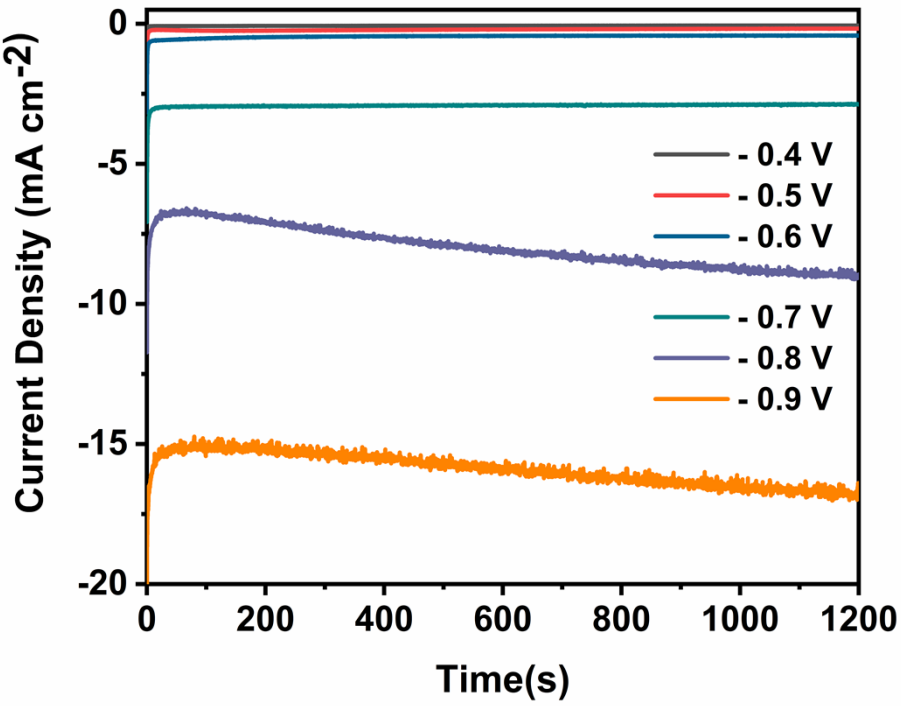

Fig. S39 Chronoamperometric responses at different potentials (*vs*. RHE) for CPOC-Ni.

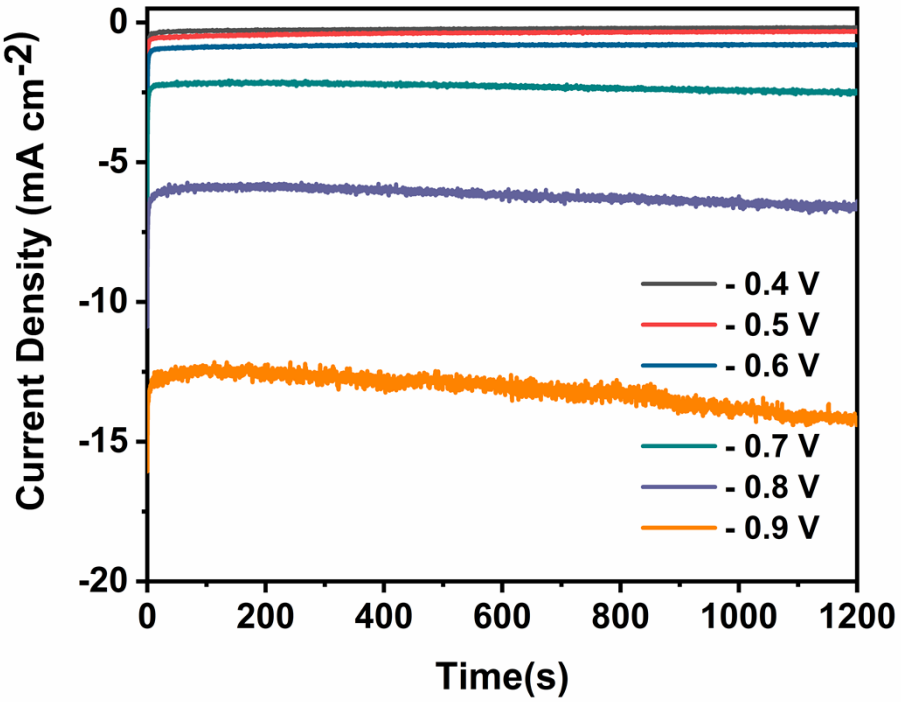

Fig. S40 Chronoamperometric responses at different potentials (*vs*. RHE) for CPOC-Cu.

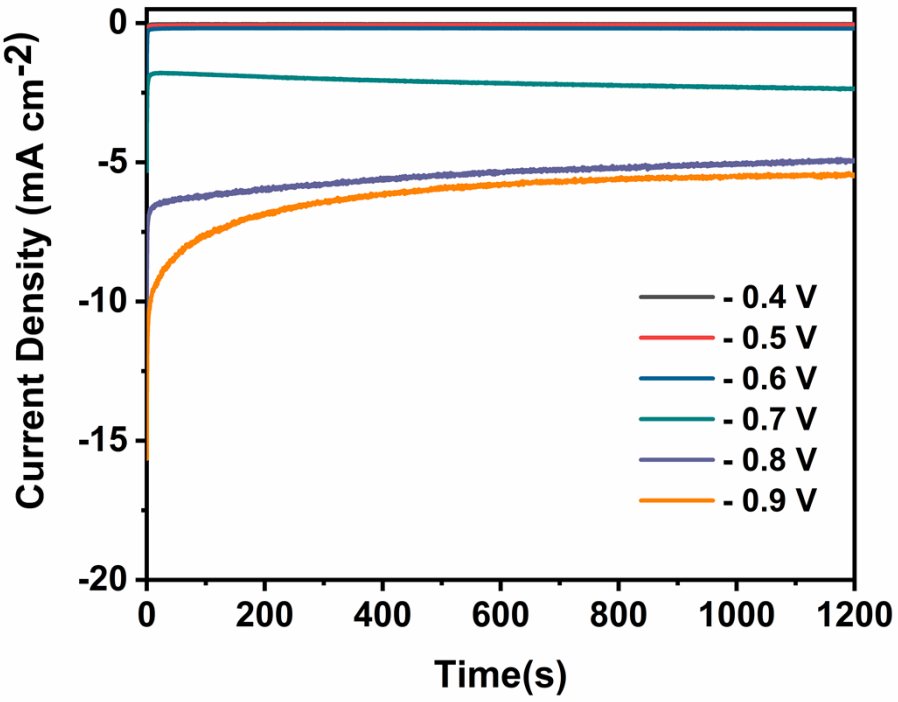

Fig. S41 Chronoamperometric responses at different potentials (*vs*. RHE) for CPOC-Zn.

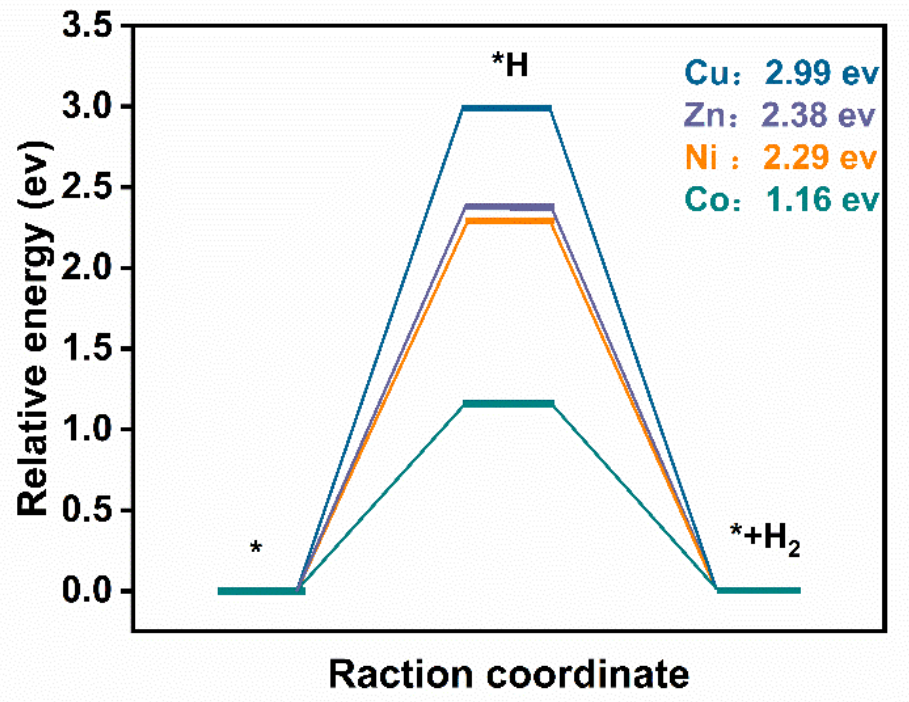

Fig. S42 Calculated Gibbs free energy diagrams for H_2O-to-H_2 conversion on four proposed active sites in Por-M.

Table S1 The corresponding BeerLambert plot recorded at different wavelength.

	λ_{max}(nm)	362	383	422	519	528	555	594	651
Molar Absorption Coefficient	TPP	/	/	370198	14780	/	6351	4807	4118
	CNDI	22532	27317	/	/	/	/	/	/
	CPOC−H_2	142703	171472	521404	33573	/	20621	12063	12046
	CPOC−Co	150163	209750	604776	/	62547	/	/	/
	CPOC−Ni	149523	199531	593426	/	55692	/	/	/
	CPOC−Cu	101759	122082	559442	/	29023	/	/	/
	CPOC−Zn	105205	124105	538328	/	32320	/	/	/

Table S2 Time constants of the corresponding species obtained from global analysis.

	ANDI	TPP	CPOC-H_2	CPOC-Co	CPOC-Zn	CPOC-Ni	CPOC-Cu
τ_{S_1}(ps)	0.3	0.2	0.2	1.6	2.0	1.3	2.5
τ_{T_1}(ps)	---	>7000	28.0	9.6	21.0	>7000	>7000

Table S2 Comparison of CPOC−Co catalyst with other electrocatalysts.

Catalysts	Structure	Type of electrolytic cell	Electrolyte	Potential (V *vs*. RHE)	FE_{CO} (%)	TON	TOF (s^{-1})	j_{CO} (mA cm^{-2})	Load of catalyst (mg/cm^2)	surface concentration of active site (mol cm^{-2})	active sites	Ref
CPOC−Co	0 D	H−cell	0.5 M aq.$KHCO_3$	−0.7	92	35128	0.98	9.9	1	8.14×10^{-8}	13.4%	This Work
CoPc−PI−COF−1	2D	H−cell	0.5 M aq.$KHCO_3$	−0.7	93	277000	2.2	9.4	1	2.2×10^{-8}	3.5%	S16
				−0.9	95	NP	4.9	21.2	1			
CoPc−PI−COF−2		H−cell	0.5 M aq.$KHCO_3$	−0.7	95	NP	1.9	6.2	1	1.7×10^{-8}	3.0%	
				−0.9	92	NP	5.0	16.6	1			
CoPc−PI−COF−3	3 D	H−cell	0.5 M aq.$KHCO_3$	−0.9	96	35500	0.6	31.7	1	1.83×10^{-7}	32.7	S17
COF−367−Co	2 D	H−cell	aq.$KHCO_3$	−0.67	91	3901	0.5	3.3	NP	1.9×10^{-8}	4%	S4
COF−366−F−Co	2 D	H−cell	0.5 M aq. aq.$KHCO_3$	−0.67	87	NP	NP	NP	NP	NP	NP	S18
Co−TTCOF	2 D	H−cell	0.5 M aq.$KHCO_3$	−0.7	91.3	141479	1.28	1.84	1	7×10^{-9}	0.9%	S19
COF−300−AR	3 D	H−cell	0.1 M aq.$KHCO_3$	−0.85	80	NP	NP	NP	NP	NP	NP	S20
CoPcPDQ−COF	2 D	H−cell	0.5 M aq.$KHCO_3$	−0.66	96	320000	3.17	22.12	1	NP	4.72%	S5
NiPc−TFPN COF−light*	2 D	H−cell	0.5 M aq.$KHCO_3$	−0.9	100	NP	0.14	17.5	1	NP	NP	S21
NiPc−COF	2 D	H−cell	0.5 M aq.$KHCO_3$	−1.1	93	NP	1.05	35	NP	NP	NP	S22
		Flow Cell	1 M aq.KOH	− 0.5 V	94.4	NP	NP	54	NP	NP	NP	
MOF−1992/CB	3 D	H−cell	0.1 M aq.$KHCO_3$	−0.63	80	5800	0.20	13.2	0.1	2.7×10^{-7}	25%	S23
CoPc−Cu−NH	2 D	H−cell	0.2 M aq.$KHCO_3$	−0.74	72	NP	1.15	8.35	NP	NP	NP	S24
CoPc−Cu−O	2 D			−0.74	85	NP	0.63	13.1	NP	9.12×10^{-8}	NP	
Co−PMOF	2 D	H−cell	0.5 M aq.$KHCO_3$	−0.80	98.7	NP	0.46	18.8	NP	NP	NP	S25
Fe−PB	0 D	H−cell	0.5 M aq. aq.$KHCO_3$	−0.63	85	55250	0.64	0.49	0.01	1.13×10^{-9}	54%	S26
COP−SA	2 D	H−cell	0.5 M aq.$KHCO_3$	−0.65	96.5	NP	46.3	8.16	9.5×10^{-4}	7.778×10^{-9}	0.876%	S27
Co−u−COF/graphene	2 D	H−cell	0.5 M aq.$KHCO_3$	−0.58	97	NP	0.92	8.2	NP	NP	NP	S28
		Flow Cell	1 M aq.$KHCO_3$	−1.15	99	NP	14	239	0.5	NP	NP	
D−P−CoPc	2 D	H−cell	0.5 M aq.$KHCO_3$	−0.61	97	NP	0.11	NP	1	NP	NP	S29
CoPc−py−CNT	0 D	H−cell	0.2 M aq.$KHCO^3$	−0.63	98.4	NP	4.9	5.5	0.046	5×10^{-9}	NP	S30
Co^{II}CPY/CNT	0 D	H−cell	0.1 M aq.$KHCO_3$	−0.7	96	NP	9.59	10.73	25 ug/cm2	5.93×10^{-8}	NP	S31
CoPc/CNT	0 D	H−cell	0.1 M aq.$KHCO_3$	−0.63	92	97,000	2.7	10	0.4	1.8×10^{-8}	NP	S32
CoPc−CN/CNT					96		4.1	15	0.4	1.8×10^{-8}	NP	

CCG/CoPc−A	0 D	H−cell	0.1 M aq.$KHCO_3$	−0.69	77	6.7×10^5	~5	1	NP	9.0×10^{-10}	NP	S33
CoPc2@MWCNTs	0 D	Flow Cell	0.5 M aq.$KHCO_3$	−0.676	93	24516	6.81	18.1	0.011	NP	NP	S34
CoPc/OxC	0 D	H−cell	0.1 M aq.NaHCO$_3$	−0.73	80	NP	113	0.34	0.01 ug/cm^2	1×10^{-11}	NP	S35
TTF−Por(Co)−COF	2 D	H−cell	0.5 M aq.$KHCO_3$	−0.9	67.2	NP	0.19	6.88	0.3	NP	NP	S36
NiPc−NiO_4	2 D	H−cell	0.5 M aq.$KHCO_3$	−1.2	NP	NP	0.72	34.5	NP	NP	NP	S37
NiPc−$Ni(NH)_4$	2 D	H−cell	0.5 M aq.$KHCO_3$	−1.1	96.4 (−0.7 V)	NP	NP	24.8	NP	NP	NP	S38
COF−366−Co@CNT	2 D	H−cell	0.5 M aq.$KHCO_3$	−0.68	92	NP	NP	6.8	0.5	NP	NP	S39
TT−Por(Co)−COF	2 D	H−cell	0.5 M aq.$KHCO_3$	−0.7	NP	NP	0.13	7.28	0.4	2.6×10^{-9}	NP	S40
NiPc–OMe MDE	0 D	H−cell	0.5 M aq.$KHCO_3$	−0.64	99.5	NP	2.9	14.5	0.4	NP	NP	S41
		Flow Cell	1 M aq.$KHCO_3$	−0.61	99.6%	NP	12	150	0.4	NP	NP	
NiPc Cage	0 D	H−cell	0.1 M aq.$KHCO_3$	−1.2 V	98.7%	NP	0.17	NP	1	NP	NP	S42

References

S1. S. Hong, M. R. Rohman, J. Jia, Y. Kim, D. Moon, Y. Kim, Y. H. Ko, E. Lee and K. Kim, *Angew. Chem. Int. Ed*., 2015, **54,** 13241-13244.

S2. T. Šolomek, N. E. Powers-Riggs, Y.-L. Wu, R. M. Young, M. D. Krzyaniak, N. E. Horwitz and M. R. Wasielewski, *J. Am. Chem. Soc.,* 2017, **139,** 3348-3351.

S3. J.-Z. Liao, L. Meng, Y.-R. Weng, J.-F. Lan, H. He, X.-H. Cheng, L. Mao, H. Ke and C.-Z. Lu, *Dyes Pigm.,* 2021, **193,** 109503.

S4. S. Lin, C. S. Diercks, Y.-B. Zhang, N. Kornienko, E. M. Nichols, Y. Zhao, A. R. Paris, D. Kim, P. Yang, O. M. Yaghi and C. J. Chang, *Science,* 2015, *349,* 1208-1213.

S5. N. Huang, K. H. Lee, Y. Yue, X. Xu, S. Irle, Q. Jiang and D. Jiang, *Angew. Chem. Int. Ed.,* 2020, **59,** 16587-16593.

S6. C. Adamo and V. Barone, J*. Chem. Phys.,* 1999, **110,** 6158-6170.

S7. G. W. T. M. J. Frisch, H. B. Schlegel, G. E. Scuseria, M. A. Robb, J. R. Cheeseman, G. Scalmani, B. M. V. Barone, G. A. Petersson, H. Nakatsuji, M. Caricato, X. Li, H. P. Hratchian, A. F., J. B. Izmaylov, G. Zheng, J. L. Sonnenberg, M. Hada, M. Ehara, K. Toyota, R. Fukuda, J. Hasegawa, T. N. M. Ishida, Y. Honda, O. Kitao, H. Nakai, T. Vreven, J. A. Montgomery, Jr., J. E. Peralta, F., M. B. Ogliaro, J. J. Heyd, E. Brothers, K. N. Kudin, V. N. Staroverov, T. Keith, R. Kobayashi, J. , K. R. Normand, A. Rendell, J. C. Burant, S. S. Iyengar, J. Tomasi, M. Cossi, N. Rega, J. M. , M. K. Millam, J. E. Knox, J. B. Cross, V. Bakken, C. Adamo, J. Jaramillo, R. Gomperts, R. E., O. Y. Stratmann, A. J. Austin, R. Cammi, C. Pomelli, J. W. Ochterski, R. L. Martin, K. Morokuma, , G. A. V. V. G. Zakrzewski, P. Salvador, J. J. Dannenberg, S. Dapprich, A. D. Daniels, O. Farkas, J. and J. V. O. B. Foresman, J. Cioslowski, D. J. Fox, Gaussian, Inc., Wallingford CT, 2013, Version D.0.

S8. P. C. Hariharan and J. A. Pople, *Teor. Chim. Acta,* 1973, **28,** 213-222.

S9. M. S. Gordon, *Chem. Phys. Lett,* 1980, **76,** 163-168.

S10. R. C. Binning Jr. and L. A. Curtiss, *J Comput Chem,* 1990, **11,** 1206-1216.

S11. D. Andrae, U. Häußermann, M. Dolg, H. Stoll and H. Preuß, *Teor. Chim. Acta,* 1990, **77,** 123-141.

S12. S. Grimme, S. Ehrlich and L. Goerigk, J *Comput Chem,* 2011, **32,** 1456-1465.

S13. I. Mayer, *Chem. Phys. Lett,* 1983, **97,** 270-274.

S14. F. L. Hirshfeld, *Teor. Chim. Acta,* 1977, **44,** 129-138.

S15. S. Yang, W. Hu, X. Zhang, P. He, B. Pattengale, C. Liu, M. Cendejas, I. Hermans, X. Zhang, J. Zhang and J. Huang, *J. Am. Chem. Soc.,* 2018, **140,** 14614-14618.

S16. B. Han, X. Ding, B. Yu, H. Wu, W. Zhou, W. Liu, C. Wei, B. Chen, D. Qi, H. Wang, K. Wang, Y. Chen, B. Chen and J. Jiang, *J. Am. Chem. Soc.,* 2021, **143,** 7104-7113.

S17. B. Han, Y. Jin, B. Chen, W. Zhou, B. Yu, C. Wei, H. Wang, K. Wang, Y. Chen, B. Chen and J. Jiang, *Angew. Chem. Int. Ed.,* 2022, **61,** e202114244.

S18. C. S. Diercks, S. Lin, N. Kornienko, E. A. Kapustin, E. M. Nichols, C. Zhu, Y. Zhao, C. J. Chang and O. M. Yaghi, *J. Am. Chem. Soc.,* 2018, **140,** 1116-1122.

S19. H.-J. Zhu, M. Lu, Y.-R. Wang, S.-J. Yao, M. Zhang, Y.-H. Kan, J. Liu, Y. Chen, S.-L. Li and Y.-Q. Lan, *Nat. Commun.,* 2020, **11,** 497.

S20. H. Liu, J. Chu, Z. Yin, X. Cai, L. Zhuang and H. Deng, *Chem,* 2018, **4,** 1696-1709.

S21. M. Lu, M. Zhang, C.-G. Liu, J. Liu, L.-J. Shang, M. Wang, J.-N. Chang, S.-L. Li and Y.-Q. Lan, *Angew. Chem. Int. Ed.,* 2021, **60,** 4864-4871.

S22. M.-D. Zhang, D.-H. Si, J.-D. Yi, S.-S. Zhao, Y.-B. Huang and R. Cao, *Small,* 2020, **16,** 2005254.

S23. R. Matheu, E. Gutierrez-Puebla, M. Á. Monge, C. S. Diercks, J. Kang, M. S. Prévot, X. Pei, N. Hanikel,

B. Zhang, P. Yang and O. M. Yaghi, *J. Am. Chem. Soc.,* 2019, **141,** 17081-17085.

S24. Z. Meng, J. Luo, W. Li and K. A. Mirica, *J. Am. Chem. Soc.,* 2020, **142,** 21656-21669.

S25. Y.-R. Wang, Q. Huang, C.-T. He, Y. Chen, J. Liu, F.-C. Shen and Y.-Q. Lan, *Nat. Commun.,* 2018, **9,** 4466.

S26. P. T. Smith, B. P. Benke, Z. Cao, Y. Kim, E. M. Nichols, K. Kim and C. J. Chang, *Angew. Chem. Int. Ed.,* 2018, **57,** 9684-9688.

S27. Y. Song, J.-J. Zhang, Z. Zhu, X. Chen, L. Huang, J. Su, Z. Xu, T. H. Ly, C.-S. Lee, B. I. Yakobson, B. Z. Tang and R. Ye, *Appl. Catal. B,* 2021, **284,** 119750.

S28. H. Gu, G. Shi, L. Zhong, L. Liu, H. Zhang, C. Yang, K. Yu, C. Zhu, J. Li, S. Zhang, C. Chen, Y. Han, S. Li and L. Zhang, *J. Am. Chem. Soc.,* 2022, **144,** 21502-21511.

S29. H. Wu, M. Zeng, X. Zhu, C. Tian, B. Mei, Y. Song, X.-L. Du, Z. Jiang, L. He, C. Xia and S. Dai, *ChemElectroChem,* 2018, **5,** 2717-2721.

S30. M. Zhu, J. Chen, R. Guo, J. Xu, X. Fang and Y.-F. Han, *Appl. Catal. B,* 2019, **251,** 112-118.

S31. L. Sun, Z. Huang, V. Reddu, T. Su, A. C. Fisher and X. Wang, *Angew. Chem. Int. Ed.,* 2020, **59,** 17104-17109.

S32. X. Zhang, Z. Wu, X. Zhang, L. Li, Y. Li, H. Xu, X. Li, X. Yu, Z. Zhang, Y. Liang and H. Wang, *Nat. Commun.,* 2017, **8,** 14675.

S33. J. Choi, P. Wagner, S. Gambhir, R. Jalili, D. R. MacFarlane, G. G. Wallace and D. L. Officer, *ACS Energy Lett.,* 2019, **4,** 666-672.

S34. M. Wang, K. Torbensen, D. Salvatore, S. Ren, D. Joulié, F. Dumoulin, D. Mendoza, B. Lassalle-Kaiser, U. Işci, C. P. Berlinguette and M. Robert, *Nat. Commun.,* 2019, **10,** 3602.

S35. M. Zhu, R. Ye, K. Jin, N. Lazouski and K. Manthiram, *ACS Energy Lett.,* 2018, **3,** 1381-1386.

S36. Q. Wu, R.-K. Xie, M.-J. Mao, G.-L. Chai, J.-D. Yi, S.-S. Zhao, Y.-B. Huang and R. Cao, *ACS Energy Lett.,* 2020, **5,** 1005-1012.

S37. J.-D. Yi, D.-H. Si, R. Xie, Q. Yin, M.-D. Zhang, Q. Wu, G.-L. Chai, Y.-B. Huang and R. Cao, *Angew. Chem. Int. Ed.,* 2021, **60,** 17108-17114.

S38. M.-D. Zhang, D.-H. Si, J.-D. Yi, Q. Yin, Y.-B. Huang and R. Cao, *Sci China Chem,* 2021, **64,** 1332-1339.

S39. Y. Lu, J. Zhang, W. Wei, D.-D. Ma, X.-T. Wu and Q.-L. Zhu, *ACS Appl. Mater. Interfaces,* 2020, **12,** 37986-37992.

S40. Q. Wu, M.-J. Mao, Q.-J. Wu, J. Liang, Y.-B. Huang and R. Cao, *Small,* 2021, **17,** 2004933.

S41. X. Zhang, Y. Wang, M. Gu, M. Wang, Z. Zhang, W. Pan, Z. Jiang, H. Zheng, M. Lucero, H. Wang, G. E. Sterbinsky, Q. Ma, Y.-G. Wang, Z. Feng, J. Li, H. Dai and Y. Liang, *Nat. Energy,* 2020, **5,** 684-692.

S42. Y. Hu, S. Huang, L. J. Wayment, J. Wu, Q. Xu, T. Chang, Y.-P. Chen, X. Li, B. Andi, H. Chen, Y. Jin, H. Zhu, M. Du, S. Lu and W. Zhang, *Cell Reports Physical Science,* 2023, **4,** 101285.